Electron-Spin-Resonance and Infrared Studies of Semiconducting, Rare-Earth-Doped CdF_2†

P. EISENBERGER AND P. S. PERSHAN*
Division of Engineering and Applied Physics, Harvard University, Cambridge, Massachusetts
(Received 31 August 1967)

Normally insulating and transparent low-doped CdF_2 becomes semiconducting and colored when baked in a Cd vapor. The electron-spin-resonance (ESR) spectrum of the semiconducting samples are compared with the insulating ones for numerous dopants. The differences found are shown to arise either from the paramagnetic "conduction" electrons themselves or from the interactions of those electrons with paramagnetic dopants. Calculations are made which explain the observed g value of 1.955 and the line-shape variations of the "conduction"-electron resonance. The properties of the observed signal in semiconducting gadolinium-doped samples are explained on the basis of a model in which the conduction electrons are coupled to the Gd^{3+} by an exchange interaction. The method of moments was used to calculate a theoretical spectrum for that system. The results are in agreement with the observed frequency of the exchange-coupled system as well as its angular dependence, which arises from the crystal-field interaction with the gadolinium. Optical studies on many differently doped samples from 50 000 to 30 cm^{-1} successfully obtain the properties of the absorption band which appears upon conversion to the semiconducting state. A broad band appears whose peak is at 0.16 eV, which agrees with the activation energy for conductivity obtained by Weller from Hall studies. However, broad wings extended into the far infrared (below 30 cm^{-1}) as well as into the ultraviolet (for 0.1% doped samples). The use of the system as a photodetector is investigated. It is found that it has potential device applications as a detector in the infrared. Initial experiments are made to specify the physical principles of its operation as well as to determine the condition for optimum performance. All the phenomena described above indicate, in different ways, the existence of localized regions in the crystal in which the "conduction" electrons have a higher mobility than the bulk mobility of the sample, and therefore such regions play a central role in the physical model developed for the system.

I. INTRODUCTION

CADMIUM fluoride, CdF_2, has the well-known fluorite structure. The fluorine atoms are on the corners of a cube with a cadmium atom at every other body-centered position. Thus the cadmium atoms have octahedral coordination with the fluorines while the fluorines have tetrahedral coordination with the cadmiums. The length of the cube is 2.725 Å, which is one-half the unit cell dimension. The pure crystal is an insulator with a resistivity of the order of 10^7 Ω cm at room temperature. It is transparent in the visible, having only a charge-transfer transition at 6 eV and a restrahlen absorption at 250 cm^{-1}. From optical studies which extended into the far infrared[1] its static and high-frequency dielectric constants are 9 and 2.37, respectively. CdF_2 can be doped with numerous trivalent dopants. Typically the trivalent rare earths are the most interesting. If the dopants are introduced into the system in the form of trifluorides, then an extra fluorine, F^-, will be in the lattice to compensate for the extra charge of each trivalent dopant present. Those extra fluorines occupy interstitial sites. In this manner over-all charge neutrality is maintained. For low-dopant concentrations, 0.1% or less, the bulk properties of the system which were described above are qualitatively unchanged by the presence of the dopant.

In 1961 Kingsley and Prenner[2] discovered that when trivalent rare-earth-doped CdF_2 is baked together with cadmium metal the insulating and transparent crystal becomes semiconducting and colored. By using the isotope Cd^{109} they were able to determine that the cadmium metal was not diffusing into the crystal.[3] By vapor-pressure studies they concluded that the conversion process involved the diffusion of the interstitial fluorines, which were compensating the trivalent dopant, to the surface where they combined with the Cd metal. Two electrons were liberated into the crystal for each CdF_2 molecule formed on the surface, and it is those electrons which are thought to provide the observed conductivities of 10 mho/cm at room temperature.

Weller[4] showed that there were two groups of dopants: The first, Nd, Sm, Gd, Tb, Dy, Ho, Er, Tm, Yb, Lu, Y, Sc, after baking, would result in a semiconductor. The second, La, Ce, Pr, Eu, and U remain insulating. No exact explanation presently exists for the inability of the second group to produce a semiconducting state after baking; however, it undoubtedly has to do with the relative stability of the oxidation states of the dopants. For those dopants that can be converted, Weller performed Hall studies.[4] His results, in general, were as follows: (1) The conductivity was n type. (2) The number of carriers initially decreased exponentially with temperature as it was lowered from room temperature. However, before reaching 77°K this decrease leveled off and began to decrease at a much

† This work was supported in part by the Joint Services Electronics Program (U.S. Army, U.S. Navy, and U.S. Air Force) under Contract Nonr-1866(16), and by the Division of Engineering and Applied Physics, Harvard University.
* Alfred P. Sloan Foundation Fellow.
[1] J. D. Axe, J. W. Gaglianello, and J. E. Scardefield, Phys. Rev. **139**, A1211 (1965).
[2] J. D. Kingsley and J. S. Prenner, Phys. Rev. Letters **8**, 315 (1962).
[3] J. D. Kingsley, J. Chem. Phys. **38**, 667 (1963).
[4] P. F. Weller, Inorganic Chem. **4**, 1545 (1965).

slower rate. Peak mobilities of 10^3 cm^2/V sec were measured at about 100°K. The quantitative results varied with the dopant used though the general properties described above were the same in all the cases studied. The general properties[2] and the low-temperature mobility behavior are characteristic of impurity banding,[5] although the initial exponential increase in the mobility can be explained by a polaron model.[6]

The semiconducting behavior contrasts with the results one gets when doped CaF_2, BaF_2, or SrF_2 are baked in the presence of their respective metals. In those hosts the trivalent dopant becomes divalent.[7] Even at 77°K, where one might have presumed the electrons were trapped at the rare-earth ion site, there was no indication of divalent ions in converted CdF_2 samples.[4] The difference can most probably be attributed to the considerably greater electron affinity of the Cd^{2+} compared to Ca^{2+}, Ba^{2+}, or Sr^{2+}.[8]

Weller,[9] in a second work, investigated this difference by growing mixed CdF_2, CaF_2 crystals doped with a trivalent dopant which could be converted in CdF_2. He found that if more than 10% CaF_2 was added the baking process failed to produce a semiconductor; however, it was not until the crystals were 99.5% CaF_2 that the trivalent dopant ions became divalent. If the dopant concentration itself was increased above 10% in CdF_2, the baking process failed to produce a semiconducting state. In fact, in both instances the change from the 0.1-Ω cm resistivities characteristic of the semiconductor to the 10^7 Ω value of the normal crystals occurred between 7 and 10% impurity concentrations. Exact explanations of these results are not known. Weller suggested one possible interpretation; however, another possibility which cannot be discounted is that the conversion process itself becomes less efficient.

After successful conversion, the normally transparent crystal becomes blueish black in color, though the exact color will vary slightly depending upon the dopant used. Weller investigated this absorption in the visible and found that it increased as λ^3 as one went further into the red. It was too large in his 0.1% doped samples to follow beyond 10 000 Å. Upon cooling to 77°K this absorption was decreased by a factor of 4, but cooling to 1.5°K caused no further reduction. The large absorption at low temperature led Weller to conclude that the absorption was not due to "free" electrons.

The objective of this work is to understand the various electronic states of these semiconducting crystals. Insight into this problem is given by electron-spin-resonance (ESR) studies in which the movement of the carriers plays a major role in determining the nature of the resonance spectra observed. These results are presented in Sec. III and are interpreted in Sec. IV. Further properties of the system are determined by optical and electrical investigations. These results are reported in Sec. V and discussed in Sec. VI. The absorption band which appears upon conversion has been shown to make the converted CdF_2 a very efficient photodetector over a very wide frequency range.[10] Its properties are presented in Sec. V; in Sec. VI they are compared to those of existing detectors.

II. EXPERIMENTAL CONSIDERATIONS

A. Sample Preparation

The samples used in this experiment were grown in graphite crucibles by use of the Bridgeman-Stockbarger technique.[11–14] The CdF_2 powder was obtained from the General Electric Chemical Products Plant. The pure powder was first purified by repeated growth of single crystals. After each growth the top end of the resultant crystal was cut off and the remainder was ground up to be used as the initial powder for the next growth. After sufficient purification, usually only two growths, the dopant was added to the pure powder and the final crystal was then grown. Spectroscopic analysis by the Jarrell-Ash Company revealed that the highest magnetic impurity apart from the dopant was Mn^{2+}, which was present in 0.001 mole % concentration. Apart from Ca, which was present in 0.008-mole % concentration, all other impurities were 0.001% or lower. The analysis also revealed that the dopant concentration in the crystal was on the order of a factor of 10 lower than the dopant concentration added to the melt.[15]

As grown the samples were highly insulating. The procedure used in these experiments to convert them into the semiconducting state is described below. A Pyrex tube was cleaned and baked under vacuum at 550°C for 2 h. The doped sample and a piece of cadmium metal were placed in the tube so that they were physically separated. The tube was then sealed and placed in a cold furnace. The temperature of the furnace was raised in 30 min to 510°C and kept there for 15 min. The tube was removed from the furnace while hot. A blueish black color was observed immediately after removing the sample from the furnace. In samples which were converted this color was slightly reduced after cooling to room temperature. In samples kept in the furnace and allowed to cool slowly a complete loss of color and conductivity occurred in some

[5] N. F. Mott and W. D. Twose, Advan. Phys. **10**, 107 (1961).
[6] H. Frohlich, Proc. Roy. Soc. (London) **A160**, 230 (1937).
[7] Z. J. Kiss, and P. N. Yocom, J. Chem. Phys. **41**, 1511 (1964).
[8] W. M. Latimer, *Oxidation Potentials* (Prentice–Hall Publishing Co., Inc., Englewood Cliffs, N.J., 1938), pp. 293–301.
[9] P. F. Weller, Inorganic Chem. **5**, 73 (1966).
[10] P. Eisenberger and P. S. Pershan, Appl. Phys. Letters **10**, 248 (1967).
[11] D. C. Stockbarger, J. Opt. Soc. Am. **39**, 731 (1949).
[12] I. V. Stepanov and P. P. Feofilov, in *Growth of Crystals*, edited by A. V. Shubnikov and N. N. Sheftal' (Consultants Bureau Inc., New York, 1959), Vol. 1, Ch. IV.
[13] J. M. Baker, W. Hayes, and D. A. Jones, Proc. Phys. Soc. (London) **73**, 942 (1959).
[14] H. Guggenheim, J. Appl. Phys. **34**, 2482 (1963).
[15] All results are labeled by the concentration added to the melt. However, the concentration actually present in the crystal can vary considerably.

instances. This was not pursued further. All samples used in these experiments were quenched in that they were taken from the furnace while it was hot. Other discussions of the conversion process can be found in the literature.[3,4] It should be noted that we originally tried to buy these crystals commercially but were unsuccessful in converting them. The cause of this failure is not known, though the presence of oxygen in place of interstitial fluorine compensation is known to affect the conversion in CaF_2 of trivalent rare-earth ions to divalent ions very markedly.[16]

B. ESR Spectrometers

Two electron-spin-resonance (ESR) spectrometers were used in these investigations. A 13-Gc/sec balanced bolometer system was used most often with some results being supplemented by the use of a commercial Varian (V4502) 35-Gc/sec spectrometer. The cavity for the 13-Gc/sec spectrometer was a rectangular TE_{102} cavity. When thin rectangular conducting samples were studied they were mounted in the middle of the cavity with the broad rectangular faces parallel to the imaginary line which divides the TE_{102} cavity into two TE_{101} cavities. This imaginary line roughly bisected the sample. For 0.1% doped[15] converted samples, conductivity of 10 mho/cm at room temperature, it was found that a loss in Q of 4 or 5 occurred for 0.010-in.-thick samples. The frequency of the cavity could be tuned by a quartz rod which could be moved in and out of the cavity. No measurements of frequency shifts due to the conducting sample were made. Great care had to be taken to center the sample in the middle of the cavity, since the smallest deviation from the central position resulted in a complete destruction of the Q of the cavity. High-density Styrofoam pieces were cut which fitted tightly into the cavity and in which a place for the rectangular sample was bored out. They were very helpful in achieving optimum location of the sample. The cavity used with the 35-Gc/sec spectrometer was cylindrical and was made by Varian (V4531). For this cavity the conducting samples were made in the form of long thin plates which were inserted along the cylindrical axis of the cavity.

III. ESR EXPERIMENTAL RESULTS

A. General Guide

When doped CdF_2 is converted, only some fraction x of the interstitial F^-'s are removed. Therefore, after conversion there are N trivalent ions, $n=xN$ "conduction" electrons and $F=(1-x)N$ interstitial F^-'s in the crystal. The distribution of the F^- interstitials in the lattice relative to the N-dopant ions is not known but ESR results obtained here, and other ENDOR studies[17] indicate that they are not nearest neighbors of the trivalent dopants. We will ignore the interstitial F^-'s for the moment. The distribution of the trivalent dopant ions relative to one another is also unknown. At different temperatures the distribution of the conduction electrons will change. Those changes will depend upon the fixed distribution of the traps (trivalent dopant ions) and the compensators (interstitial F^-'s). This will be discussed further in Sec. VI.

We will interpret the experiments to be described here in terms of three general types of configurations. The first of these is the isolated dopant by which is meant a dopant site which is basically identical to a site in the unconverted crystal. That is, there is no "conduction electron" near it. The second configuration consists of groups of two or more dopants which are near enough to each other that an electron can move (or tunnel) rather "freely" between them. The size of these groups, their spacial distribution, and the number of electrons with which they are interacting can vary considerably. For the concentration of dopants employed in these experiments it is likely that the mean dopant-dopant distance for these groups is considerably smaller than would be obtained from a random distribution of ions throughout the crystal. The third configuration consists of an isolated trivalent rare-earth ion which has an electron near it. The two are presumed to be interacting with each other. The actual distributions of electrons among these various configurations will certainly depend on temperature and on concentration of dopants. In reality there is probably a continuum of configurations which connect the three cases described above.

The physical properties of these configurations vary and the different experimental results to be discussed below will be interpreted in terms of these variations.

B. ESR of Dopants in Uncovered CdF_2

1. *Diamagnetic Dopants*

The diamagnetic trivalent dopants that were investigated in detail were Lu^{3+}, Y^{3+}, La^{3+}. These ions have filled $4f$, $4p$, $5p$ shells, respectively. ESR of these diamagnetic samples at room temperature, 77°K, and 1.5°K revealed only resonances due to the Mn^{2+} impurity.

2. *Gadolinium (Gd^{3+})*

The electronic configuration of Gd^{3+} is $4f^7$ which has a $^8S_{7/2}$ ground state. In a cubic crystalline field the octet ground state is split into doublets (Γ_6, Γ_7) and one quartet (Γ_8). The ESR spectrum has been measured at room temperature in CaF_2 by Low[18] and in CdF_2 by Baker and Williams.[19] The appropriate spin

[16] J. Merz, Phys. Rev. (to be published).
[17] R. Borscherts (private communication).
[18] W. Low, Phys. Rev. **105**, 265 (1958).
[19] J. M. Baker and F. I. B. Williams, Proc. Roy. Soc. (London) **78**, 1340 (1962).

TABLE I. Spin-Hamiltonian parameter for Gd^{3+} in CdF_2 and CaF_2. c and d in cm^{-1}.

Temperature	CdF_2 [a] R.T.	77°K	1.5°K	CdF_2 [b] R.T.	CaF_2 [c] R.T.
c	0.0173±0.0005	0.0203±0.0005	0.0205±0.0005	0.0190±0.0005	0.0185±0.0005
d	0.0000±0.0002	0.0000±0.0002	0.0000±0.0002	0.0000±0.0005	−0.0004±0.0002
g	1.992±0.002	1.992±0.001	1.992±0.001	1.992±0.002	1.0991±0.002

[a] This work. [b] Baker and Williams (Ref. 19). [c] Low (Ref. 18).

Hamiltonian for a cubic field can be written as[19]

$$\mathcal{H}=g\beta\mathbf{H}\cdot\mathbf{S}+B_4(O_4^0+5O_4^4)+B_6(O_6^0-21O_6^6), \quad (3.1)$$

where the O_n^m are operator equivalents in the notation of Baker *et al.*,[20] and B_4, B_6 characterize the strength of the cubic-crystalline field. To determine the exact resonance spectrum for any arbitrary orientation of the magnetic field is very difficult in this case since the crystal-field terms and the Zeeman term are the same order of magnitude.[19] However, to the required accuracy perturbation theory is sufficient to determine the resonance spectrum as one varies the magnetic field. The calculation was carried out by Low[18] and we simply quote his result below

Transition	Frequency
$\pm\frac{7}{2}\rightleftharpoons\pm\frac{5}{2}$	$g\beta H\pm\frac{1}{2}(10c+3d)\rho+\epsilon_1$
$\pm\frac{5}{2}\rightleftharpoons\pm\frac{3}{2}$	$g\beta H\mp\frac{1}{2}(5c+7d)\rho+\epsilon_2$
$\pm\frac{3}{2}\rightleftharpoons\pm\frac{1}{2}$	$g\beta H\mp\frac{1}{4}(12c-17d)\rho+\epsilon_3$
$+\frac{1}{2}\rightarrow-\frac{1}{2}$	$g\beta H+\epsilon_4$.

Here $c=240B_4$, $d=5040B_6$; ϵ_1, ϵ_2, ϵ_3, and ϵ_4 are functions of $c^2/g\beta H$, $d^2/g\beta H$, and $cd/g\beta H$. Also, $\rho=1-5\phi$, $\phi=l^2m^2+m^2n^2+l^2n^2$, where l, m, n are the direction cosines between the magnetic field and the cubic axis. The spectrum observed as the magnetic field is varied in the (100) plane is shown in Fig. 1. This spectrum was measured at room temperature, 77°K, and 1.5°K. The observed angular dependence agrees with the perturbation results. The values obtained for the parameters g, c, d, are given in Table I, where they are compared to those found by other investigators. The 15% increase in c at 77°K over room temperature is probably due to the shrinking of the lattice. The important feature of the spectrum for the purposes of this study is the crossing point, 32° from ⟨100⟩ directions, when the seven transitions become roughly degenerate. The resonance condition at the crossing point ($\rho=0$) is given by $h\nu=g\beta H$, where g is the spectroscopic splitting factor which was found to be $g=1.992\pm0.002$, as is shown in Table I.

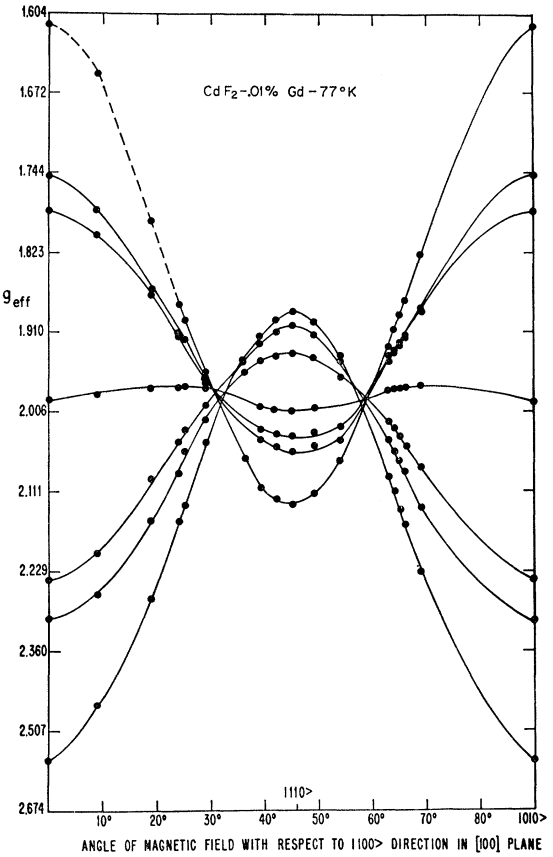

FIG. 1. Angular variation of unconverted Gd^{3+} spectrum.

3. *Ytterbium (Yb)*

The electronic configuration of Yb^{3+} is $4f^{13}$ which has a $^2F_{7/2}$ ground state. In a cubic field the $S=\frac{7}{2}$ level is split as in Gd^{3+} into doublets $[\Gamma_6, \Gamma_7]$ and one quartet $[\Gamma_8]$. However, since $L\neq0$ the crystal-field splittings are much larger than the Zeeman term. The ESR spectrum[21] indicates that the Γ_7 doublet is lowest. The cubic spin Hamiltonian has an effective spin of $\frac{1}{2}$. In addition, Yb has nuclear isotopes Yb^{171} ($I=\frac{1}{2}$, 19.3%) and Yb^{173} ($I=\frac{5}{2}$, 16.9%) which cause a hyperfine splitting of the Zeeman transitions. The ESR resonance spectrum of Yb^{3+} has been investigated in CdF_2 by

[20] J. M. Baker, B. Bleaney, and W. Hayes, Proc. Roy. Soc. (London) **247**, 273 (1958).

[21] W. Low, Phys. Rev. **118**, 1608 (1960).

TABLE II. Spin-Hamiltonian parameters for Yb^{3+} in CdF_2 and CaF_2.

Constant	Frequency measured (Mc/sec)	CdF_2 [a]	CdF_2 [b]	CaF_2 [c]
g	9 117	...	3.4359±0.0008	3.426±0.001
g	13 170	3.433±0.001	...	...
g	31 149	...	3.4308±0.0005	...
g	72 179	...	3.4171±0.0006	...
A_{171}	...	$882\pm2\times10^{-4}$ cm^{-1}	$883\pm1.5\times10^{-4}$ cm^{-1}	$886\pm1.5\times10^{-4}$ cm^{-1}
A_{173}	...	$241\pm1\times10^{-4}$ cm^{-1}	$242\pm0.4\times10^{-4}$ cm^{-1}	$243.2\pm0.4\times10^{-4}$ cm^{-1}

[a] This work. [b] Konyukhov (Ref. 22). [c] Low (Ref. 21).

Konyukhov *et al.*,[22] and in CaF_2 by Low.[21] The spin Hamiltonian is[22]

$$\mathcal{H}=g\beta\mathbf{H}\cdot\mathbf{S}+A_{171}\mathbf{S}\cdot\mathbf{I}_{171}+A_{173}\mathbf{S}\cdot\mathbf{I}_{173}. \quad (3.2)$$

The spectroscopic splitting factor g is magnetic-field-dependent due to the admixture of the excited Γ_8 state into the ground state. Its value is given by[22]

$$g=3g_J[1-4(g_J\beta H/3\gamma)^2], \quad (3.3)$$

where $g_J=\frac{8}{7}$ is the appropriate free-atom value for a $^2F_{7/2}$ level and where γ is the energy separation between the Γ_7 and Γ_8 levels. The values obtained for the spin-Hamiltonian parameters in the unconverted samples are given in Table II, where they are compared to those found by other workers. These measurements were made at 1.5°K; above 20°K the resonance is too broad to observe.

C. Converted Samples

1. Diamagnetic Dopants

The three diamagnetic dopants investigated were Lu^{3+}, Y^{3+}, and La^{3+}. Since La^{3+} samples do not become semiconducting after baking[4] they were used as a standard to insure that the baking process itself, independent of the transition to the semiconducting state, did not produce any paramagnetic states. ESR results on La^{3+} at room temperature, 77°K, and 1.5°K before and after baking revealed identical results. Only a signal due to the Mn^{2+} impurity was observed.

In both Lu^{3+} and Y^{3+} after conversion an additional resonance appeared. This resonance was observed in 0.01% Y, 0.3% Y, and 0.06% Lu samples.[15] The g factor for both types of dopants was 1.955±0.005. The 0.3% Y sample[15] was measured at room temperature and 77°K on 13 Gc/sec and 35 Gc/sec spectrometers. The g values found were as follows: $g_{13\,\mathrm{Gc/sec}}^{300°\mathrm{K}}=1.960\pm0.005$; $g_{35\,\mathrm{Gc/sec}}^{300°\mathrm{K}}=1.950\pm0.005$; $g_{13\,\mathrm{Gc/sec}}^{77°\mathrm{K}}=1.960\pm0.005$; $g_{35\,\mathrm{Gc/sec}}^{77°\mathrm{K}}=1.953\pm0.005$. The line shape at room temperature for a 0.010-in.-thick sample is shown in Fig. 2. It has the characteristic Dysonian shape for the case that the skin depth is smaller than the thickness of the sample. It should be noted that the ratio of the two peaks (A/B) is 2.7±0.1 at 13 Gc/sec and 2.7±0.1 at 35 Gc/sec. This will be of some use in calculating the diffusion time of the carriers. By 77°K the line shape was Lorenztian and the half-width had increased. At helium temperatures the line shape still appeared to be Lorenztian though the presence of the Mn^{2+} impurity made an exact determination of the shape difficult. It was possible, though very difficult, to saturate the signal at 1.5°K. The variation of the linewidth and integrated intensity with temperature is shown in Table III. The intensity was measured relative to the Mn^{2+} impurity in the sample. The blank spaces in Table III arise for the 0.01% Y sample[15] because, at 1.5°K, the large linewidth caused the signal to be too weak to measure accurately. The 1.5°K measurement for the Lu sample was not made. The general result is that the intensity remained constant, but the linewidth increased with decreasing temperature. Spectroscopic analyses of the 0.3% Y sample[15] revealed that the ratio of Y^{3+} to Mn^{2+} was 30. From Table III the ratio of conduction electrons to Mn^{2+} is found to be three. This seems to indicate that only 10% of the interstitial F^-'s are removed ($x=\frac{1}{10}$) or

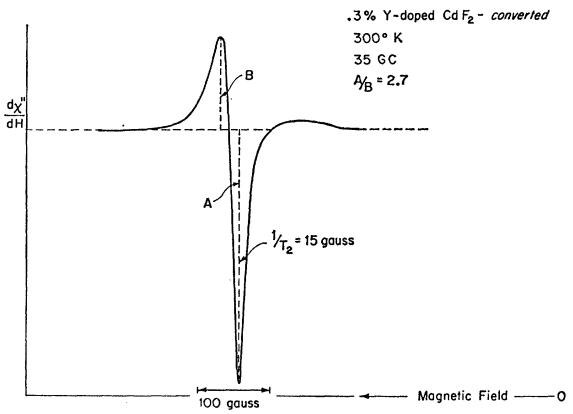

FIG. 2. Line shape of "conduction" electrons' resonance.

[22] V. K. Konyukhov, P. P. Pashinin, and A. M. Prokhorov, Fiz. Tverd. Tela 4, 246 (1962) [English transl.: Soviet Phys.—Solid State 4, 175 (1962)].

TABLE III. Intensity and linewidth variation with temperature of $g=1.955$ signal for 0.3% Y, 0.01% Y, 0.06% Lu samples (Ref. 15). R=ration of $g=1955$ signal to Mn^{2+} signal. The latter was normalized to correspond to the signal of one of the five Mn^{2+} electrons.

Temperature (°K)	0.3% Y $R(\pm 0.2)$	0.3% Y Width (G)	0.01% Y $R(\pm 0.2)$	0.01% Y Width (G)	0.06% Lu $(R\pm 0.2)$	0.06% Lu Width (G)
300	3	15	1	15	3	15
77	3	38	1	38	3	40
1.5	3	100	...	...	...	...

for some reason not all the electrons are observable by ESR. The latter, for example, arising out of the differentiation of properties depending on whether the electron is trapped at configuration 2 or 3 of our gross classification. However, the former seems more likely since Weller[7] made a similar observation about the conversion process from his conductivity studies. It is quite certain that the conversion efficiency can vary considerably with the condition of the surface of the sample being a vital factor. This may possibly explain why the 0.01% Y signal[15] was only $\frac{1}{3}$ that of the 0.3% Y signal.[15] Qualitative measurements were made between 77 and 1.5°K on the linewidth. There was a distinct leveling off in the increasing width as one approached 1.5°K.

2. *Gadolinium* (Gd^{3+})

Since Gd^{3+} is paramagnetic the possibility of magnetic interaction between the electrons and Gd^{3+} ions in configurations 2 and 3 exists. The nature of this interaction will be discussed in Sec. IV B. For the converted Gd^{3+} samples very striking changes were observed. In general, the significant change was the appearance of an "eighth" absorption line as the magnetic-field orientation approached the crossing point, shown in Fig. 1, from any direction.[23] This is also shown in Fig. 3. Note especially that the other seven Gd^{3+} transitions do not change in intensity as the "eighth" signal grows.

Orienting the crystal so that the magnetic field was in the [100] plane, the derivative traces shown in Fig. 4 were obtained as the magnetic field was varied towards the crossing point at 32°. These plots only include a blown up section of the region near the central transition so that the growth of the "eighth" signal could be clearly seen. The other six transitions are approaching the crossing point as the magnetic field is varied in the exact same manner as in the unconverted sample (Fig. 1).

At room temperature, when one is far from the crossing point, no signal at all is observable. As the crossing point is approached, however, the "eighth resonance" appears. This is shown in Fig. 3, where the resonance spectrum of the converted sample is plotted as a function of the magnetic field orientation. Note that at crossing (32°) the gain is $\frac{1}{10}$ what it was 8° away from crossing. The spectrum was monitored continuously as the sample was allowed to warm up from 77°K to room temperature. A continuous change from the spectrum shown in Fig. 4 to that shown in Fig. 5

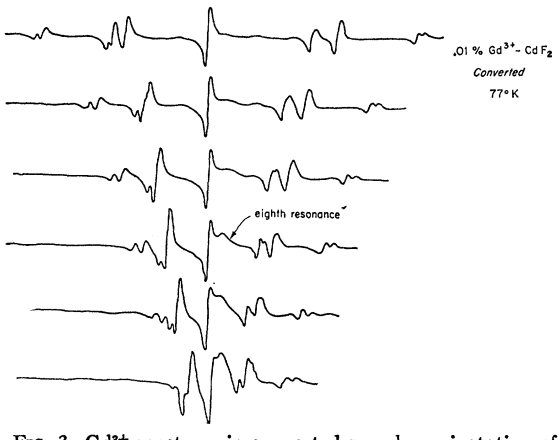

FIG. 3. Gd^{3+} spectrum in converted sample—orientation of magnetic field varied in a nonprincipal plane.

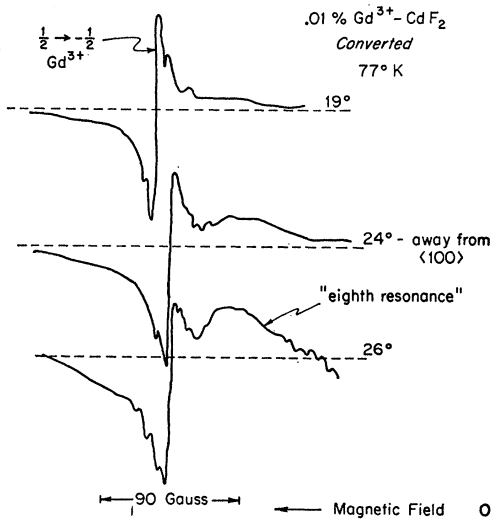

FIG. 4. Central portion of converted Gd^{3+} spectrum. Orientation of magnetic field varied in [100] plane (77°K).

[23] P. Eisenberger and P. S. Pershan, Bull. Am. Phys. Soc. **12**, 416 (1967).

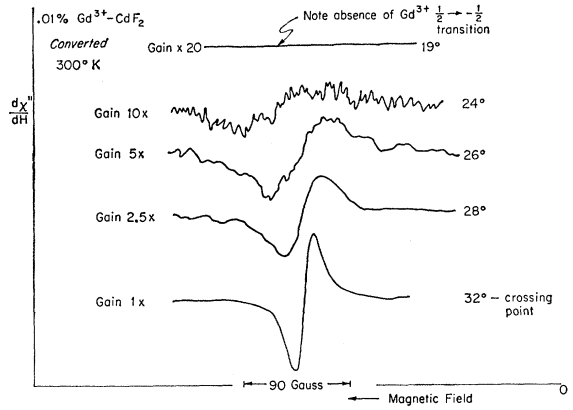

FIG. 5. Converted Gd^{3+} spectrum. Orientation of magnetic field varied in [100] plane (room temperature).

was observed. In this same temperature range the resistivity of the sample decreases from 500 Ω cm to 0.1 Ω cm. The variation, with angle, of the peak-to-peak derivative height of the "eighth" absorption is shown in Fig. 6 for room temperature. Note the exact parallel in symmetry between that plot and Fig. 1, which shows the crystal-field splittings as a function of angle. The integrated intensity of the "eighth" absorption was roughly independent of the angle from crossing until one was more than 7° away, beyond which a sharp decrease was noticed. The "eighth" absorption was centered at a g value of 1.992 ± 0.001, which is coincident, within the experimental error, with the g value of Gd^{3+}.

The intensity of the "eighth resonance" relative to the unaffected Gd^{3+} spectrum changed with temperature as is obvious from Figs. 4 and 5. This change was measured relatively and absolutely. The absolute measurement was obtained by comparing the observed intensities in a converted and unconverted sample which were equal in volume and dopant concentration. The latter follows since the two pieces were cut from the same piece of a large single crystal. The accuracy of this measurement was ascertained by the repeatability of the results for each individual measurement. The relative measurement was taken by measuring this ratio both when the magnetic field was oriented along the [100] direction and at the crossing point. The results for 0.01% Gd-doped samples[15] are given in Table IV. The room-temperature results are only relative, because of the finite skin depth and lower Q of the cavity for the conducting sample. They have been normalized by comparing the observed signal in the two samples to the Mn^{2+} signal in those samples. Similar qualitative results were obtained for 0.005% and 0.1% Gd^{3+}-doped samples.[15] The low-doped sample showed a higher percentage of unaffected Gd^{3+} sites at all temperatures than the more highly doped samples.

The weak intensity of the unaffected Gd^{3+} spectrum at room temperature made accurate measurement of the intensity and line shape of the eighth absorption possible. However, at lower temperatures, as is clear from Fig. 3, the unaffected Gd^{3+} spectrum made such measurements impossible.

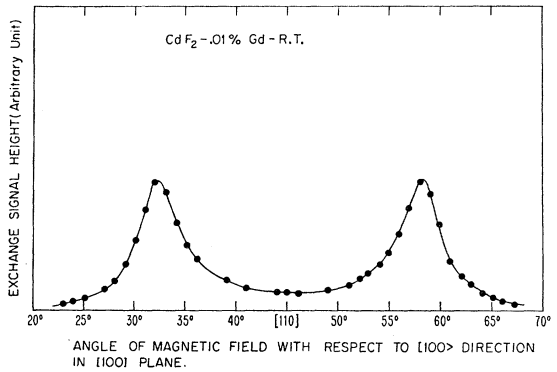

FIG. 6. Peak-to-peak derivative height of "eighth" resonance (exchange signal) as a function of magnetic field orientation in [100] plane.

TABLE IV. Comparison of the intensity of converted to unconverted 0.01% Gd (Ref. 15). r_1 = ratio measured with magnetic field along [100], r_2 = ratio measured 32° from [100] (the crossing point).

Temperature (°K)	0.01% Gd $r_1(\pm5\%)$	$r_2(\pm5\%)$
300	0	0.24
300[a]	0.01<	~1
77	0.27	1.05
1.5	0.60	1.02

[a] Normalized to Mn^{+} + signal.

The failure to observe any resonance near $g=1.955$, the value characteristic of the free electron, suggests that the "eighth" resonance may be due to the coupled electron Gd^{3+} spectrum. This will be discussed in Sec. IV. B.

The unaffected Gd^{3+} spectrum observed in the converted samples at 77°K and 1.5°K had the identical frequency splitting as a function of orientation as in the converted sample. The only difference between the two spectra was in their relaxation times. Those differences were illustrated by saturation studies made at 1.5°K. The results are shown in Fig. 7. The increased relaxation rate of the Gd^{3+} in the converted sample is indicated in those figures by the higher power necessary to make the signal deviate from its ideal response indicated by the straight line. An increase in relaxation rate is exactly what one would expect due to the additional relaxation mechanism provided by the interaction with the moving paramagnetic electron.

3. *Ytterbium (Yb)*

A 0.01%-doped Yb sample[15] from the same boule as the crystal used to obtain the results for the uncon-

verted sample was converted. Its signal at 1.5°K was compared to the unconverted sample. The spectrum was characterized by the same spin Hamiltonian (3.2) with the parameters having the same values (Table II). However, the intensity was diminished by 30%. We will discuss the cause of this loss in intensity further in Sec. IV C. We merely note for the present that for Gd^{3+}, when the magnetic field was oriented away from crossing at 1.5°K, there was a loss of 40% in the ratio of the intensity of the converted sample to that of the unconverted sample. As in the case of Gd_2 the unaffected Yb in the converted sample had a faster relaxation rate than the Yb in the unconverted sample. The experimental saturation curves are shown in Fig. 8.

4. *Terbium* (Tb^{3+})

The spectra of Tb^{3+}-doped crystals was looked at in both the converted and unconverted state. No comparative intensity measurements were made; however, no new signals appeared in the converted sample. The region near $g=1.955$ was looked at very closely.

IV. DISCUSSION

A. Diamagnetic Dopants

1. *g Value*

Since Cd^{2+} has a filled $4d$ shell the extra electron added to form Cd^{+} ion should be in a $5s$ orbital. In a tight-binding model, this would suggest that the bottom of the CdF_2 conduction band should be primarily S-like. On the other hand, it it were pure S-like the free-electron g value should be very close to the pure spin value of 2.002. Experimentally, the "conduction" electron g value in CdF_2 is significantly different ($g=1.955$). The usual correction to g values arise from spin-orbit coupling. However, for these contributions to be nonzero, one must first have some non $L=0$

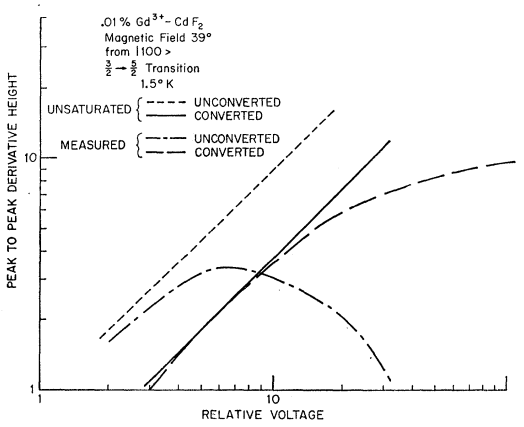

FIG. 7. Signal intensity as a function of incident microwave field. Converted and unconverted 0.01% Gd; magnetic field along |100>.

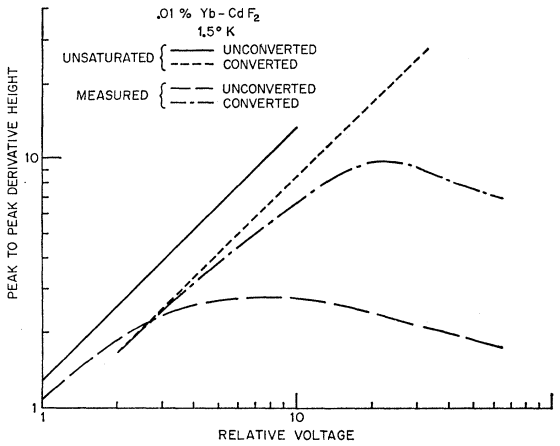

FIG. 8. Signal intensity as a function of incident microwave field. Converted and unconverted 0.01% Yb.

states mixed into the wave function of the electron so that even though $L\Psi=0$, $L_z^2\Psi\neq 0$. In what follows an attempt will be made to show how such wave functions can get mixed into the mainly $5s$-type wave function of the free electrons.

There is at present no band-structure information concerning the CdF_2 lattice. In view of this and the ionic nature of CdF_2 lattice, localized wave functions were used to describe the "free" electron. That is, we will analyze the state of the electron located at a point $\mathbf{R}_i$ in the lattice in terms of the localized Cd wave functions which are near $\mathbf{R}_i$. Strictly speaking, one should allow for some fluorine-type wave functions; however, rough estimates suggest these effects should be much smaller than the ones to be described. For the moment we will neglect fluorine-type orbitals. This will be justified below. The use of localized orbitals is the familiar LCAO approach, where in this case, one will be using the Cd $5s$ and $5p$ wave functions to expand our "free"-electron's wave functions. This approach is not strictly correct[24]; however, for the purposes of this calculation no serious error should be introduced. Considering $\mathbf{R}_i$ to coincide with a Cd^{2+} site one can then write the wave function for the electron using only Cd^{2+} atomic orbital states as

$$\Psi(\mathbf{R}_i)=\alpha\Psi_{\mathrm{Cd}\,5s}(\mathbf{R}_i)+\sum_{j=1}^{N}\beta_j\Psi_{\mathrm{Cd}\,j}(\mathbf{R}_i-\mathbf{a}_j), \quad (4.1)$$

where the displacement vector a_j connects the central Cd site at $\mathbf{R}_i$ to its 12 nearest-neighbor Cd sites 3.85 Å away, its 8 next-nearest neighbor sites 5.45 Å away, etc. The constant β_j is therefore the envelope of our expansion, and as is clear, determines the spread of the electron's wave function. We will limit our sum to the twelve nearest neighbors since these contributions should be the greatest, though as will be clear from

[24] J. M. Ziman, *Principles of the Theory of Solids* (Cambridge University Press, London, 1966), p. 84.

calculation more distant neighbors are easily included. Thus, the wave function becomes

$$\Psi(\mathbf{R}_i)=\alpha\Psi_{\mathrm{Cd}\ 5s}(\mathbf{R}_i)+\beta\sum_{j=1}^{12}\Psi_{\mathrm{Cd}\ j}(\mathbf{R}_i-\mathbf{a}_j)/(\alpha^2+12\beta^2)^{1/2}, \tag{4.2}$$

where α, β are a measure of the distribution of the electronic charge between the central Cd^{2+} site and each of its 12 nearest neighbors. One expects that $\alpha>\beta$ and thus the outer Cd^{2+} sites will find themselves polarized. This distortion will result in the appropriate wave functions for the nearest neighbors having the form

$$\Psi_{\mathrm{Cd}\ j}(\mathbf{R}_i-\mathbf{a}_j)=(1+\epsilon^2)^{-1/2}$$
$$\times[\Psi_{\mathrm{Cd}\ 5s}(\mathbf{R}_i-\mathbf{a}_j)+\epsilon\sum_{l=1}^{3}a_{jl}\Psi^{l}{}_{\mathrm{Cd}\ 5p}(R_i-\mathbf{a}_j)], \tag{4.3}$$

where ϵ is a measure of the distortion and the linear combination of cadmium $5p$ wave functions is chosen so as to represent the electronic polarization of the wave functions towards the central ion. The appropriate linear combination for each of the 12 sites is shown in Appendix A. It is clear that such linear combinations have the desired effect of introducing terms in the wave function of the electron for which $L_z=0$ but $L_z^2\neq 0$.

It has been shown by Adrian[25] in connection with the F-center problem that

$$\Delta g=-2\sum(\langle\Psi\mid\lambda l_{iz}^2\mid\Psi\rangle/\Delta E), \tag{4.4}$$

where ΔE is the $5s$ to $5p$ energy separation and where λ is the Cd^{+} spin-orbit parameter. The l_{iz} operator is centered at the site on which it operates.[25] The usual form of the spin-orbit corrections has the same $\lambda/\Delta E$ dependence.[26] For the element Cd the values of ΔE and λ are $+3.85$ eV and $+0.212$ eV, respectively.[27] These values can change slightly for Cd in CdF_2, but this change should not be large. Using the wave functions from Appendix A, it is easily shown that neglecting overlap

$$\Delta g=-\frac{2\lambda}{\Delta E}\frac{\epsilon^2}{(1+\epsilon^2)}\frac{\beta^2}{\alpha^2+12\beta^2}\,28/3, \tag{4.5}$$

which, using our values of λ and ΔE and $\alpha^2+12\beta^2=1$ and $\epsilon^2<1$, becomes

$$\Delta g\simeq-3\epsilon^2\beta^2. \tag{4.6}$$

The measured value of Δg was 0.047 and therefore a value of $\epsilon^2\beta^2\cong 0.016$ would be required. This is consistent with our assumption of small polarization and a larger charge density on the central Cd ion than on the 12 neighbors. Actually ϵ^2 and β^2 are related, since the larger the charge on the central ion (i.e., the smaller β) the larger the distortion (ϵ). Therefore, in fact, the quantity $\epsilon^2\beta^2$ is the physically interesting one and is a measure of the polarized charge at the nearest-neighbor sites. The effect of increasing the number of neighbors considered would be an expansion of Δg of the form

$$\Delta g=-2\lambda(\Delta E)^{-1}[(28/3)\epsilon_1^2\beta^2+4\epsilon_2^2\beta_2^2+\cdots], \tag{4.7}$$

where each succeeding $\epsilon_1^2\beta_1^2$ would be smaller. It is the large value of the spin-orbit parameter which accounts for the fact that a small admixture of p-type states can produce such a relatively large g shift.

The invariance of the g factor, for free electrons in Lu^{3+}- and Y^{3+}-doped crystal, with their considerably different spin-orbit parameters, suggests strongly that the g value is a property of the bulk lattice and not of the dopant.

2. Line Shape

The changing width and shape of the resonance signal for Yb^{3+} and Lu^{3+} dopants arises from separate but related phenomena. The shape at room temperature is the well-known Dysonian line shape for paramagnetic ions in a conducting medium.[28] Using the measured dc conductivity of 10 mho/cm for the 0.3% Y-doped sample,[15] whose line shape was shown in Fig. 3, the calculated skin depth δ was 10^{-4} cm at room temperature for the 35-Gc/sec radiation used. From the ratio of A to B in Dyson's theory, one can determine the ratio of the width of the line $1/T_2$, to the time, T_D, it takes the carriers to diffuse a distance equal to the skin depth. The ratio 2.7 measured for the $g=1.955$ signals indicates that $T_D/T_2>4$. Thus, even a stationary paramagnetic ion, $T_D=\infty$, would have the same shape. This is verified by examining the line shape of the Mn^{2+} impurities. However, it can be easily shown that for the 0.3% Y-doped samples[15] that $T_D/T_2>4$ is not a very great restriction on the motion of the electrons. The measured value for the line width $(1/T_2)$ was 2×10^8 sec^{-1}. Thus T_D must be greater than 2×10^{-8} secs. Given Dyson's formula for T_D[28]:

$$T_D=3\delta^2Ne^2/2\sigma m^*v^2, \tag{4.8}$$

where N is the concentration of carriers which is roughly 10^{18}/cm^3, m^* is the effective mass which will be taken equal to the free mass, and where v is the average velocity of the electrons, and using our values, one finds that the velocity v must not be greater than 0.5×10^7 cm/sec for the line shape to have the ratio $A/B=2.7$. For the low carrier concentrations the Maxwell-Boltzmann statistics can be used and the thermal velocity at room temperature is 10^7 cm/sec. Thus, the observed line shape is not inconsistent with that expected for a moving carrier. The alkali metals investigated by Feher had an A/B ratio which was 1.5 to 5 times greater than the 2.7 value measured here.[29] The larger ratio indicated that T_D/T_2 was 0.1 or less.

[25] F. J. Adrian, Phys. Rev. **107**, 488 (1957).
[26] W. Low, in Solid State Abstr., Suppl. 2, 44 (1962).
[27] Y. Yafet, Solid State Phys. **14**, 8 (1963).
[28] F. J. Dyson, Phys. Rev. **98**, 349 (1955).
[29] G. Feher and A. F. Kip, Phys. Rev. **98**, 332 (1955).

A small T_D is expected for a fast-moving carrier. The differences between the alkali metals and the CdF_2 semiconductor are that the Fermi velocity is greater than the thermal velocity of Maxwell-Boltzmann statistics and the Fermi mean free path is larger than the mean free path in CdF_2. Thus, if the frequency for which the metal is measured is adjusted so that the skin depth is the same for the two cases the time T_D will be greater in CdF_2 than in the alkali metals.

We have until now ignored the admixture of fluorine orbitals into our wave function. This is justified in the calculation of the g factor, since the spin-orbit parameter is much smaller for the lighter elements. For example, $\lambda \cong 0.01$ eV for nitrogen.[27] However, in considering the linewidth and shape the fluorine orbitals must be included due to their large nuclear-magnetic moment.

In addition to the fluorine contribution, there is also a small but finite admixture of the dopant's wave function depending upon the amount of time the electron spends in the vicinity of a dopant and how strongly it interacts with the dopant. It will be asserted later that this admixture is related to the exchange interaction between the electrons and the dopants when the dopants are paramagnetic.

Taking the above considerations into account, a wave function can be written which has the form

$$\Psi = \alpha' \Psi_{\mathrm{Cd}} + \beta' \Psi_{\mathrm{F}} + \delta' \Psi_{\mathrm{dopant}}, \tag{4.9}$$

where $\alpha' > \beta' > \delta'$ are phenomenological constants. An appropriate spin Hamiltonian for this case of diamagnetic dopants would be

$$\mathcal{H} = \sum_i g_i \beta \mathbf{H} \cdot \mathbf{S}_i + \sum_{ij} a_{ij} \mathbf{S}_i \cdot \mathbf{I}_j = \mathcal{H}_z + \mathcal{H}_{\mathrm{hf}}, \tag{4.10}$$

where S_i is the spin of the ith electron, I_j is the nuclear spin of the jth fluorine and a_{ij} is the hyperfine interaction constant. If the electron were localized at one site, one could consider the case of an isolated electron and allow the sum over j to include the nearby fluorines. For the simplest case of only the eight nearest neighbors and an isotropic hyperfine interaction, the spectrum would consist of nine discrete transitions. Each of these nine transitions is characterized by the total z-component of the nuclear spin of the eight surrounding fluorines. In the average spectra for many sites, each of the nine transitions would have a relative strength proportional to the number of ways the total

$$I^z = \sum_{j=1}^{8} I_j^z$$

could be achieved. The splitting between these nine lines would be a_j. The second moment is easily calculated[30] and can take the form

$$\Delta H^2 = \tfrac{1}{3} \sum_{j=1}^{8} |\, a_j \,|^2 I_j (I_j + 1), \tag{4.11}$$

where $I_j = \frac{1}{2}$. A general expression for a_j would be rather complicated but it would have the form $a_j = (8\pi/3) g_F^2 \beta_F \,|\, \Psi_{ej} \,|^2$, where $|\, \Psi_{ej} \,|^2$ is, in some sense, the density of the electronic-wave function at the jth fluorine site.

If, however, the electron is moving our Hamiltonian becomes

$$\mathcal{H} = \mathcal{H}_z + \mathcal{H}_{\mathrm{hf}} + \mathcal{H}_m, \tag{4.12}$$

where $\mathcal{H}_m$ represents the kinetic energy of the electron. As the electron moves its hyperfine local field will be changing since the fluorine nuclear-spin orientations differ from site to site; however, the Zeeman energy is unchanged. Thus,

$$[\mathcal{H}_z, \mathcal{H}_m] = 0 \quad \text{but} \quad [\mathcal{H}_{\mathrm{hf}}, \mathcal{H}_m] \neq 0. \tag{4.13}$$

This is the familiar case of motional narrowing[31] where it has been shown the resulting second moment is given by[31]

$$\Delta\omega_{\mathrm{motional}} = (\Delta\omega_{\mathrm{hf}})^2 \tau_c, \tag{4.14}$$

where $\Delta\omega_{\mathrm{hf}}$ is given by Eq. (4.11) and τ_c is the correlation time of the local hyperfine field. A rough estimate of τ_c for our case is the time it takes an electron to move a distance equal to its wave packet's extension in space, which we have assumed in our g-factor calculation to be on the order of 10 Å. If the electron travels over the short 10 Å distance with something like its thermal velocity, one finds using Eqs. (4.11) and (4.14) that an a_j of 6000 G is required for $\Delta\omega_{\mathrm{motional}}$ to be equal to the 15-G linewidth which was observed at room temperature. This seems physically unreasonable. An alternative mechanism for the width is relaxation-time broadening. Various relaxation mechanisms exist.

It was shown in the discussion of the g factor that the polarization caused by the electron introduced p-type wave functions into the electronic wave function. This admixture will provide a coupling to the lattice which could result in a fast relaxation time. It has been shown by Elliot[32] that

$$T_1 = \alpha[\tau_R / \Delta g^2], \tag{4.15}$$

where α is a numerical factor smaller than one and τ_R is the usual relaxation time obtained from resistivity measurements; $\Delta g = g - 2.0023$ is the deviation of the electronic g value from the free value due to spin-orbit coupling. Thus, our large Δg will result in a short T_1. Since α and τ_R are unknown for our system, a numerical estimate cannot be made, however, the large g shift which arose from the large spin-orbit parameter of Cd does give, qualitatively at least, support for a relaxation broadening mechanism at room temperature.

The increasing linewidth with decreasing temperature might be explained by assuming the slower moving electron could interact more strongly with the lattice.

[30] J. J. Markham, Solid State Phys. **8**, 224 (1966).

[31] P. W. Anderson, J. Phys. Soc. Japan **9**, 316 (1954).

[32] R. J. Elliot, Phys. Rev. **96**, 266 (1954); **96**, 280 (1954).

However, lifetime broadening is not likely since the 100-G-wide line could be saturated.

At lower temperatures, with numerous dopant traps, it becomes unreasonable to still assume that the electron travels on the average with something like its thermal velocity. The large increase in resistivity of the sample from 500 Ω cm at 77°K to 10^8 Ω cm at 1.5°K during which time the concentration of carriers remains constant,[4] is positive evidence that the trapping time will become important at these lower temperatures. Thus the correlation time will effectively become the trapping time which can be quite long. The linewidth at lower temperature could possibly be explained on the basis of either the fluorine hyperfine interaction or some interaction with the impurity. The importance of the motion even at temperatures below 77°K is suggested by the increasing linewidth with decreasing temperature and the Lorenztian shape of the line. Since neither the hyperfine constant a_j nor the trapping time τ_c are known, it is impossible to say anything quantitatively on the basis of our results. For a reasonable hyperfine field of 400 G the trapping time at 1.5°K would be $\tau_c=4\times10^{-11}$ sec if Eq. (4.14) is used. Since $\tau_{c(\text{thermal})}(1.5°\text{K})=1.5\times10^{-13}$ sec, this would mean that the electron spends more than 99% of its time trapped. An electron hopping between various dopant sites might have such properties.

B. Gd^{3+}—Eighth Resonance

There are four things to notice about the eighth resonance: (a) its existence; (b) its g value; (c) its line-shape variation with angle; and (d) its variation with temperature. The first two properties can be made plausible by considering the Hamiltonian appropriate for the converted Gd^{3+} sample with the magnetic field oriented in the crossing direction, including exchange coupling between the mobile electrons and Gd^{3+}. For the moment we merely postulate such an interaction, noting that a phenomenological basis for it was given in the previous section. After having analyzed its consequences, we will return to discuss its physical reality.

The Hamiltonian is

$$\mathcal{H}=a\sum_i S_{1i}{}^z+b\sum_j S_{2j}{}^z+\sum_{ij}J_{ij}\mathbf{S}_{1i}\cdot\mathbf{S}_{2j}, \qquad (4.16)$$

where the symbols are defined as follows: $a=g_{\text{Gd}}\beta H$, $b=g_e\beta H$, $S_{1i}{}^z$ is the z component of the ith Gd^{3+} spin, $S_{2j}{}^z$ is the z component of the jth electron spin, J_{ij} is the exchange constant between the ith electron and the jth Gd^{3+}. Thus, the first two terms are the Zeeman energies of the system, while the last is the exchange interaction. The case of interest in this study is when $|J|>|a-b|$. The case $|J|<|a-b|$ is well known. It was first treated by Van Vleck.[33] Basically his result is that the exchange coupling broadens the resonances of the two systems. It contributes a term to the linewidth on the order of J.

[33] J. H. Van Vleck, Phys. Rev. **74**, 1168 (1948).

For the case $|J|>|a-b|$, however, the two types of spins are coupled together such that the frequencies of the actual magnetic resonance lines is not obvious. Following Van Vleck[33] or Pryce and Stevens[34] one can always calculate, by use of commutation and trace relations, the values of the first, second, and higher moments of the magnetic-resonance spectrum. The complication results from the fact, first shown by Van Vleck, that often the line shape is not a simple Lorenztian or Gaussian and the lower moments are not sufficient to actually describe the observed spectrum. Van Vleck's solution to this was to truncate part of the Hamiltonian.

In this case, however, the problem is more complex since it is not obvious what operator one should use in the commutation relationships. The rigorous, or complete, moments should be calculated using $a'S_1{}^+ + b'S_2{}^+=g_{\text{Gd}}\beta\sum_i S_{1i}{}^+ + g_e\beta\sum_j S_{2j}{}^+$; however, this would include two types of transitions. For the first $J\mathbf{S}_1\cdot\mathbf{S}_2$ is conserved and the transition frequency is independent of J. Taking $\mathbf{S}=\mathbf{S}_1+\mathbf{S}_2$, these transitions conserve $\mathbf{S}_1\cdot\mathbf{S}_1$, $\mathbf{S}_2\cdot\mathbf{S}_2$, and $\mathbf{S}\cdot\mathbf{S}$. If a' were equal to b', these would be the only kind of allowed transitions. For $a'\neq b'$ there are also allowed transitions which do not conserve the exchange energy and with frequencies that can vary by as much as $\pm J$. This latter type of transition will cause a broad background signal which is not experimentally observable. The observed central line is entirely due to transitions of the first type. The problem is to separate the magnetic-moment operator into two parts, one of which will give the central line and the other the broad background.

Since $S^+=S_1{}^+ + S_2{}^+$ commutes with the exchange interaction the central linewidth will be described by an operator like $\tilde{\mu}^+=\delta S^+$. The total magnetic moment operator is given by $\mu^+=\tilde{\mu}^+ + \mu'^+$. One can easily demonstrate the existence of a sum rule[35]

$$\int f(\omega)\,d\omega = \operatorname{Tr}(\mu^+\mu^-)$$
$$= \operatorname{Tr}[\tilde{\mu}^+\tilde{\mu}^- + \mu'^+\mu'^- + \tilde{\mu}^+\mu'^- + \mu'^+\tilde{\mu}^-]. \qquad (4.17)$$

If μ'^+ is chosen such that

$$\operatorname{Tr}(\tilde{\mu}^+\mu'^-) = \operatorname{Tr}(\mu'^+\mu^-) = 0, \qquad (4.18)$$

one has two separate sum rules. The ratio of the intensity of the central component to that of the broad background is thus simply given by

$$\mathcal{R} = \operatorname{Tr}(\tilde{\mu}^+\tilde{\mu}^-)/\operatorname{Tr}(\mu'^+\mu'^-). \qquad (4.19)$$

In Appendix B it is shown how such a division is accomplished. Here we will merely quote two of the

[34] M. H. L. Pryce and K. W. H. Stevens, Proc. Phys. Soc. (London) **A63**, 36 (1950).

[35] C. P. Slichter, *Principles of Magnetic Resonance* (Harper and Row, Inc., New York, 1963), pp. 51–52.

important results from that Appendix:

(1) $\tilde{\mu}^+=[(\theta a'+b')/(1+\theta)]S^+$,

$\mu'^+=[(a'-b')/(1+\theta)](S_1^+-\theta S_2^+)$,

where $\theta=N_{\rm Gd}S_{\rm Gd}(S_{\rm Gd}+1)/N_eS_e(S_e+1)$ and $N_{\rm Gd}$, N_e are the number of Gd^{3+} and electrons, respectively. (2) The ratio of the intensity in the central component to the broad background is given by

$$\Re=[a'(\sqrt{\theta})+b'/\sqrt{\theta}]^2/(a'-b'). \tag{4.20}$$

An important aspect, particular to our problem, is that $\theta>1$, since $N_{\rm Gd}>N_e$ and $(S_{\rm Gd}=\frac{7}{2})>(S_e=\frac{1}{2})$. $\theta>1$ is the mathematical statement that the intensity contribution of the electron-spin system is small compared to the Gd^{3+} and thus the properties of the observed resonance will be mainly Gd in character. From Eq. (4.20) using $a'-b'=0.04\beta$, and $a'=2\beta$ (β is the Bohr magneton),

$$\Re\sim 2.5\times 10^3(\theta^{-1}+\theta+2).$$

Since $\theta>1$, there is a negligible fraction of the intensity in the broad signal for our system. The division we have made above can also be understood by considering Anderson's[31,36] approach to the problem of exchange narrowing. In the spirit of the previous discussion our Hamiltonian (4.16) can be rewritten

$$\mathcal{H}=\frac{(a\theta+b)}{1+\theta}S^z+\sum_{ij}J_{ij}\mathbf{S}_{1i}\cdot\mathbf{S}_{2j}+\frac{(a-b)}{1+\theta}(S_1^z-\theta S_2^z). \tag{4.21}$$

The above division is exact and completely general (Appendix B). Consider the extreme case of very large θ. Equation (4.21) becomes

$$\mathcal{H}=aS^z+\sum_{ij}J_{ij}\mathbf{S}_{1i}\cdot\mathbf{S}_{2j}-(a-b)S_2^z, \tag{4.22}$$

or symbolically

$$\mathcal{H}=\mathcal{H}_0+\mathcal{H}_{\rm ex}+\mathcal{H}_p. \tag{4.23}$$

The smallness of the last term is due both to the small value of $a-b$ and the small possible values of S_2^z compared to those of S^z. From Eq. (4.22) and the definitions of $\tilde{\mu}^+$ and μ'^+ the following are easily shown to hold:

$$[\mathcal{H}_0,\mathcal{H}_{\rm ex}]=0, \tag{4.24}$$

$$[\mathcal{H}_{\rm ex},\mathcal{H}_p]=(b-a)\sum_{ij}J_{ij}[S_{1i}^+S_{2j}^z-S_{2j}^+S_{1i}^z], \tag{4.25}$$

$$[\mu^+,\mathcal{H}_{\rm ex}]=[\tilde{\mu}^+,\mathcal{H}_{\rm ex}]+[\mu'^+,\mathcal{H}_{\rm ex}]; \tag{4.26}$$

since $[\tilde{\mu}^+,\mathcal{H}_{\rm ex}]=0$, one has

$$[\mu^+,\mathcal{H}_{\rm ex}]=[\mu'^+,\mathcal{H}_{\rm ex}]=(a'-b')\sum_{ij}J_{ij}[S_{1i}^+S_{2j}^z-S_{1i}^zS_{2j}^+]. \tag{4.27}$$

[36] P. W. Anderson, Rev. Mod. Phys. **25**, 269 (1953).

Anderson's arguments demonstrate that when the conditions (4.23)–(4.27) are satisfied $\mathcal{H}_p$ is effectively averaged out by a "strong enough" $\mathcal{H}_{\rm ex}$. In this case the average of $\mathcal{H}_p$ is nonzero but small. Since $[\mu^+,\mathcal{H}_{\rm ex}]=i\mu^+(\hbar=1)$ Eq. (4.27) says that for large J, the precession frequency of μ^+ will have a rapid time dependence and therefore the absorption will have a broad spectral distribution. However, the rapid time dependence of μ^+ arises solely from its μ'^+ component. Thus, this component will result in a broad background while the $\tilde{\mu}^+$ component will represent the transitions at $\bar{\omega}$.

Using the division of the magnetic moment discussed above the first moment or average frequency of the narrowed line is given by[33,34] ($\hbar=1$)

$$\langle\omega\rangle=\mathrm{Tr}\tilde{\mu}^-[\mathcal{H},\tilde{\mu}^+]/\mathrm{Tr}(\tilde{\mu}^-\tilde{\mu}^+). \tag{4.28}$$

From the well-known trace relationships,[33] the result is easily found to be

$$\langle\omega\rangle=(a\theta+b)/(1+\theta). \tag{4.29}$$

This is the expected result that the average frequency will be the weighted average of the two resonance frequency with the weighting factor proportional to the intensity of the individual resonances. Since $\theta=21N_{\rm Gd}/N_e$, which is much greater than 1, the average frequency for our case becomes $\bar{\omega}=a+(b-a)/\theta$. Taking a conservative estimate of one third for $N_e/N_{\rm Gd}$, one finds $\bar{g}=g_{\rm Gd}-0.0007$. The resonance therefore occurs coincident, within the experimental error, with the resonance frequency of the Gd^{3+} at crossing. This is in complete accord with our previous statement that the observed resonance should be mainly Gd^{3+} in character. It is interesting to note that the calculations in Appendix B show that the broad background spectrum is not centered near the Gd^{3+} resonance frequency but at the electron-resonance frequency.

The definition of the second moment can be written as[34]

$$\langle\omega^2\rangle=\frac{\mathrm{Tr}[\tilde{\mu}^-([\mathcal{H},[\mathcal{H},\tilde{\mu}^+]])]}{\mathrm{Tr}[\tilde{\mu}^-\tilde{\mu}^+]}, \tag{4.30}$$

which can also be written in the form[33]

$$\langle\omega^2\rangle=\frac{\mathrm{Tr}[\tilde{\mu}^-,\mathcal{H}][\mathcal{H},\tilde{\mu}^+]}{\mathrm{Tr}[\tilde{\mu}^-\tilde{\mu}^+]}. \tag{4.31}$$

Again in a straightforward manner,

$$\langle\omega^2\rangle=(a^2\theta+b^2)/(1+\theta), \tag{4.32}$$

and where from Eq. (4.29)

$$\langle\Delta\omega^2\rangle=\langle\omega^2\rangle-\langle\omega\rangle^2=(a^2\theta+b^2)/(1+\theta)-(a\theta+b/1+\theta)^2, \tag{4.33}$$

which for $\theta\gg1$

$$\langle\Delta\omega^2\rangle=(a-b)^2/\theta. \tag{4.34}$$

The third moment can be written in the spirit of Eqs. (4.28) and (4.30) as

$$\langle\omega^3\rangle=\frac{\mathrm{Tr}\{\tilde{\mu}^-[\mathcal{H},(\mathcal{H},[\mathcal{H},\tilde{\mu}^+])]\}}{\mathrm{Tr}[\tilde{\mu}^-\tilde{\mu}^+]}. \quad (4.35)$$

Again by straightforward methods,

$$\langle\omega^3\rangle=(a^3\theta+b^3)/(1+\theta), \quad (4.36)$$

which when used in

$$\langle\Delta\omega^3\rangle=\langle\omega^3\rangle-3\bar{\omega}\langle\Delta\omega^2\rangle-\bar{\omega}^3 \quad (4.37)$$

results for $\theta\gg1$ in

$$\langle\Delta\omega^3\rangle=(b-a)^3/\theta. \quad (4.38)$$

Finally the fourth moment is defined as[33]

$$\langle\omega^4\rangle=\frac{\mathrm{Tr}(\{\mathcal{H},[\tilde{\mu}^-,\mathcal{H}]\}\{\mathcal{H},[\mathcal{H},\tilde{\mu}^+]\})}{\mathrm{Tr}[\tilde{\mu}^-\tilde{\mu}^+]}, \quad (4.39)$$

which is easily shown for our Hamiltonian to be equal to

$$\langle\omega^4\rangle=(a^4\theta+b^4)/(1+\theta)+(a-b)^2J^2, \quad (4.40)$$

where $J^2=\frac{1}{3}(1/N_{\mathrm{Gd}})\sum_{ij}J_{ij}^2S_e(S_e+1)$.
Since

$$\langle\Delta\omega^4\rangle=\langle\omega^4\rangle-6\bar{\omega}^2\langle\Delta\omega^2\rangle-4\bar{\omega}\langle\Delta\omega^3\rangle-\bar{\omega}^4, \quad (4.41)$$

one finds for $\theta\gg1$

$$\langle\Delta\omega^4\rangle=(a-b)^4/\theta+(a-b)^2J^2. \quad (4.42)$$

If $J>a-b$, one notices that the fourth moment given above is larger than the square of the second moment, Eq. (4.34). In fact, the condition $J>(a-b)/\theta$ seems sufficient. For this case numerous calculations have shown[31,36,37] that one can approximate the resulting line by a Lorenztian shape in the center with a half-width given by

$$\Delta\omega_{\mathrm{ex}}=\eta\langle\Delta\omega^2\rangle^{3/2}/\langle\Delta\omega^4\rangle^{1/2}, \quad (4.43)$$

but which decreases more rapidly than $(\omega-\bar{\omega})^{-3}$ in the wings. The constant η varies depending on the theory utilized; however, it never differs greatly from unity. Using this definition our exchange width becomes by Eqs. (4.34) and (4.42)

$$\Delta\omega_{\mathrm{ex}}=(a-b)^2/J\theta^{3/2}. \quad (4.44)$$

The actual observed width at crossing will also have a contribution due to relaxation-time broadening. As discussed in Sec. IV A 2, the conduction electron had a natural linewidth at room temperature of 15 G. With paramagnetic dopants the relaxation time of the combined system could easily be fast enough to give a significant contribution to the observed linewidth. Thus, the total observed width at crossing will be given by

$$\Delta\omega_T=\Delta\omega_{\mathrm{rel}}+\Delta\omega_{\mathrm{ex}}. \quad (4.45)$$

The linewidths are added in this way since the distributions are assumed to be Lorenztian.

To calculate the variation of linewidth with magnetic field orientation it is necessary to include the crystal field terms in the Hamiltonians. In addition, to get a correct expression for the linewidth at crossing one must include dipole interactions between the electrons and Gd^{3+}. Hyperfine interactions of the fluorines with the Gd^{3+} which are responsible for the observed width of the Gd^{3+} resonances in the unconverted samples must also be included. Linewidth contributions which affect the electron alone can be safely ignored since as we have seen from our previous analysis these will contribute negligibly to the observed width since the electron contribution to the observed intensity is small. Including these contributions the Hamiltonian becomes

$$\mathcal{H}=\mathcal{H}_0+\sum[l(S_{1i}^z)^2+m(S_{1i}^z)^4]+\sum_{ij}B_{ij}S_{1i}^zS_{2j}^z+\sum_{is}a_{is}S_{1i}^zI_s^z. \quad (4.46)$$

The first term includes all those in Eq. (4.16) with the addition of that part of the dipole term which can be written in the same form as the exchange term. The second term is the crystal-field term where $l=f_1c\rho$ and $m=f_2c\rho$; c and ρ are defined in Sec. III B 2, and $f_1=-179/96$ and $f_2=14/96$ were obtained by matching the Gd^{3+} spectra to the form of the second term. Only the fourth-order contribution to the crystalline potential is included, since the sixth-order constant was shown to be vanishingly small (Table II). The third term is the dipole interaction between the electron and the Gd^{3+} ions which has the well-known form

$$B_{ij}=-3g_eg_{\mathrm{Gd}}\beta^2[\tfrac{3}{2}\delta_{ij}-\tfrac{1}{2}]/r_{ij}^3. \quad (4.47)$$

The fourth term is the hyperfine-interaction term between the Gd^{3+} and the fluorines when I_s^z are the z component of the fluorine nuclear spins and a_{is} if the Fermi contact parameter. Note that we have truncated these last two terms so that only diagonal contributions are included. This is the usual Van Vleck[33] type of truncation. Numerous calculations[31,33,36,37] exist for handling the dipole and hyperfine fields in the presence of exchange. The crystal-field term behaves in a similar manner. None of these contribute to the first moment, since their mean is zero. The crystal-field split Gd^{3+} lines are, to first order, symmetric around the central unsplit $\frac{1}{2}\rightarrow-\frac{1}{2}$ transition (Fig. 1). Thus, the first moment is as shown in Eq. (4.18), which for $\theta>1$

$$\langle\omega\rangle=a+(b-a)/\theta. \quad (4.48)$$

For the second moment each term in our Hamiltonian equation (4.38) contributes separately and thus one can with slight alterations use the usual results[37,33,31] for the hyperfine term and the dipole term. The crystal-field term has been evaluated by Bersohn.[38]

[37] A. Abragam, *Principles of Nuclear Magnetism* (Clarendon Press, Oxford, England, 1961), pp. 435–439.

[38] R. J. Bersohn, J. Chem. Phys. **20**, 1505 (1952).

One therefore finds that

$$\langle\Delta\omega^2\rangle=(a-b)^2/\theta+\langle\Delta\omega^2\rangle_{\text{c.f.}}+\langle\Delta\omega^2\rangle_{\text{dipole}}+\langle\Delta\omega^2\rangle_{\text{hf}}, \tag{4.49}$$

where, using Bersohn's results but our values of l and m,

$$\langle\Delta\omega^2\rangle_{\text{c.f.}}=9\rho^2c^2. \tag{4.50}$$

This is a reasonable result since $3\rho c$ is the average splitting of the Gd^{3+} lines from the central unsplit $\frac{1}{2}\rightarrow-\frac{1}{2}$ transition.

The dipole term is given by

$$\langle\Delta\omega^2\rangle_{\text{dipole}}=2\sum_{ij}B_{ij}^2S_e(S_e+1)/3N_{\text{Gd}} \tag{4.51}$$

and the hyperfine term has the form

$$\langle\Delta\omega^2\rangle_{\text{hf}}=\tfrac{1}{3}\sum_s a_s^2I^s(I^s+1). \tag{4.52}$$

In computing the fourth movement the hyperfine and dipole terms will be ignored since they are negligible compared to the crystal-field contributions and to the $(a-b)^2J^2$ term which, from our previous analysis, we know will be present.

An evaluation of traces shows that the fourth moment is roughly given by

$$\langle\Delta\omega^4\rangle=(a-b)^4/\theta+(a-b)^2J^2+c_1\langle\Delta\omega^2\rangle_{\text{c.f.}}^2+c_2\langle\Delta\omega^2\rangle_{\text{c.f.}}J^2. \tag{4.53}$$

The constants c_1 and c_2 are both greater than one and less than five. Their exact value depends on the evaluation of complex traces. The form of Eq. (4.53), $c_1\langle\Delta\omega^2\rangle^2+c_2\langle\Delta\omega^2\rangle J^2$ is the standard form for the fourth moment in the presence of exchange.[31,33,36]

Using Eqs. (4.43) and (4.53) under the condition $(\sqrt{c_2})J>3\rho c$ one finds

$$\Delta\omega_{\text{exch}}=\frac{[(a-b)^2/\theta+\langle\Delta\omega^2\rangle_{\text{hf}}+9\rho^2c^2+\langle\Delta\omega^2\rangle_{\text{dipole}}]^{3/2}}{J[(a-b)^2+9c_2\rho^2c^2]^{1/2}}. \tag{4.54}$$

The total linewidth will be given by Eq. (4.45). From the data one can estimate that N_{Gd}/Ne was larger than the value of 3 used previously; thus $(a-b)^2/\theta<600$ $(\text{G})^2$ at 13×10^9 cps and $\langle\Delta\omega^2\rangle_{\text{hf}}=225$ G^2. Neither of these contributions are large enough in the presence of exchange to explain the observed linewidth of 14 G at crossing, $\rho=0$. Therefore, either the dipole contribution or the relaxation term must be large. For a dipole contribution to explain the observed width, $\langle\Delta\omega^2\rangle_{\text{dipole}}$ must equal approximately $(70)^2$ $(\text{G})^2$ if the exchange field is to be of the order of 250 G. The fact that 250 G is a reasonable value for the exchange field follows from the fact that the integrated intensity of the eighth resonance remains constant only so long as $(\sqrt{c_2})J>3\rho c\sqrt{c_1}$. This will be discussed below. In view of the motion of the electrons it seems unlikely that the dipole field can be this large. The relaxation linewidth can explain the observed linewidth of 14 G.

TABLE V. Angular variation of linewidth of "eighth" resonance.

Angle	ρ	ΔH_{obs} (±2 G)	$\Delta H_{\text{theor.}}$[a]	$3\rho c/2J$
32°	0	14.4	14.4	0
31°	0.025	15.2	15.1	0.03
30°	0.065	18	18	0.08
29°	0.105	25	23	0.12
28°	0.14	32	30	0.17
27°	0.18	38	34	0.21
26°	0.225	45	47	0.27
25°	0.27	53	60	0.32
24°	0.32	63	82	0.4

[a] $J=250$; $c_2=4$; $\Delta H_{\text{rel}}=13.6$.

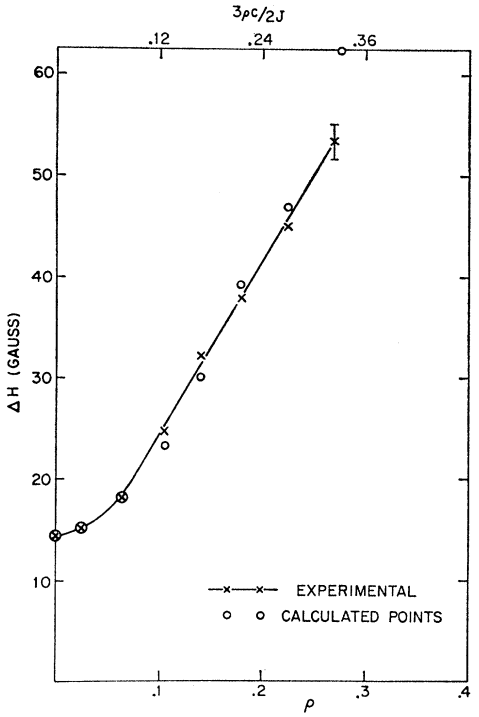

FIG. 9. Angular variation of linewidth of "eighth" resonance.

Equation (4.54) was used to evaluate $\Delta\omega_{\text{exch}}$ as a function of ρ with the results given in Table V, and plotted in Fig. 9. For these results J was chosen to be 250 G, $c_2=4$, and $\Delta\omega_{\text{rel}}=13.6$ G. The proportionality between $\Delta\omega_T$ and the peak-to-peak derivative width was taken as unity. For a Lorenztian line shape this is not correct; however, the correction is not warranted in view of the uncertainties in the definition of $\Delta\omega_{\text{exch}}$. One sees from Table V and Fig. 9 that the theory is in good agreement with the observed variation except for the last two values in Table V. However, the effective-exchange field $(\sqrt{c_2})J$ is no longer large compared to $3\rho c$ and thus Eq. (4.43) is no longer valid. Experimentally, it was observed that for $\rho>0.25$ the derivative of the absorption decreases much more rapidly in

the peak to peak height then it increases in the square of the peak-to-peak width. For $\rho<0.25$, the product (height)$\times$(width)^2 was roughly constant. This is in fact the expected result since as $(\sqrt{c_2})J$ becomes comparable to $3\rho c$ the absorption intensity is transferred from the central region at $\bar{\omega}$ to the various crystal-field split lines. The central Lorenztian approximation is no longer valid. Each of those individual transitions would, as discussed for the case $a-b>J$, have a width proportional to J which would have been too broad to observe.

A theoretical calculation of the magnitude of the constant J is not possible at the present. However, certain of the phenomenological properties involved in the determination of J are clear from our experimental results.

Firstly, the sum $(\sum_j J_{ij}^2)$ is not independent of i, the Gd^{3+} ion. There are some Gd^{3+} which are effectively decoupled from the electrons such that $\sum_j J_{ij}^2$ is zero. Those Gd^{3+} account for the "unaffected" Gd^{3+} spectrum. Secondly, the electrons are coupled to more than one Gd^{3+} ion. This is clearly shown at room temperature by the absence of any "unaffected" Gd^{3+} ions in spite of the fact that there are fewer electrons than Gd^{3+}. That various Gd^{3+} sites must be coupled together by the same electron is clearly shown by calculating the spectrum of an isolated Gd^{3+} electron pair. There would be some narrowing of the spectra in the sense of reducing the crystal-field splittings, but this reduction would never, even for very large J, reduce those splittings by a factor more than 2. The results observed in these experiments could never be explained by such a reduction. Even at helium temperatures 40% of the Gd^{3+} were coupled to the electrons. From the results on the Y-doped samples as well as Weller's result[4] the ratio of electrons to dopants seems to be about $\frac{1}{10}$, though it certainly will vary from case to case. This would indicate that even at helium temperatures an average electron sees four or more Gd^{3+} sites.

These results strongly suggest that there exist regions in the crystal even at helium temperatures where the electron is "free" to move with a mobility greater than the bulk mobility of the sample. The meaning of free will be discussed further in Sec. VI. However, in the Y^{3+} studies one concept of free arose in the explanation of the linewidth of the resonance, namely that of an electron hopping between dopant sites though spending 99% of its time trapped near those sites. Such an explanation would be equally appropriate here. For such a case the J_{ij} would then really represent the time average of the exchange interaction of the ith Gd^{3+} with the jth electron, with the interaction being large when the two are close together, but zero when they are apart. In this connection one should note that an electron-electron exchange interaction could be added to the phenomenological Hamiltonian without altering the main result.

Further support for the existence of these regions was the observance of the decrease in the magnitude of the "eighth" resonance as the concentration of the sample was reduced. The probability for Gd^{3+} ions being within a distance R of one another, as well as the hopping mobility, would decrease with decreasing concentration.

At crossing, because of the presence of free electrons, the absorption intensity in the converted sample might be larger than in the unconverted sample. But the broad background caused by the difference in g values results in a net loss of intensity in the converted sample. The calculation of Appendix B show that this should be vanishingly small. The data (Table IV) showed a slight increase; however, the uncertainties of the measurements would allow either conclusion to be drawn.

For those Gd^{3+} for which the sum $\sum_j J_{ij}^2$ is zero, the linewidth should be the same as in the unconverted sample except for the additional dipole term. This term can provide a relaxation mechanism for the Gd^{3+} ions and thus account for the faster relaxation rate of the Gd^{3+} in the converted sample.

In conclusion it can be fairly definitely stated that the eighth resonance can arise from an exchange coupling between the electrons and the Gd^{3+} ions. The nature of this coupling and its magnitude can not be explained from first principles; however, the phenomenologically obtained value for $(\sqrt{c_2})J$ of 500 G seems reasonable. The model developed for calculating the effect of the exchange is crude in the sense that it is not quite clear that $\Delta\omega_{c.f.}(t)$ is well approximated by a Gaussian random process as was tacitly assumed in the use of Eq. (4.43). In fact, it may be as we discussed in the hopping model, that the actual process occurring is that when an electron and a Gd^{3+} ion interact the various states get mixed due to the $J_{ij}S_{1j}^{+}S_{2j}^{-}$ type terms. These random variations in the Gd^{3+} wave function will modulate the Gd^{3+} precession frequency. If these variations occur fast enough an exchange averaging can occur; however, the basic form would be Markovian and not necessarily Gaussian. Anderson[36] has studied this case extensively and shown that the basic result has the same form as for the Gaussian case, $\Delta\omega_{exch}\cong\langle\Delta\omega^2\rangle/J$; however, the quantitative results may differ from one approach to another. Thus, although the magnitude of J found here is consistent and physically reasonable within the framework of its use in the phenomenological calculation, an extrapolation to a physical parameter would require a closer study of the actual interaction. The form of the interaction would then govern the statistical approach to apply in studying its effect on the line shape.

C. Yb^{3+}

The experimental results obtained for Yb^{3+} support those that we have just discussed for Gd^{3+}. The spectroscopic splitting factor of Yb^{3+} is 3.433, which differs

greatly from the 1.955 of the electron and its spin is only $\frac{1}{2}$. An analysis similar to that carried out for Gd^{3+} would show that those Yb^{3+} coupled to the electrons would be broadened out with a resultant width on the order of J. This case is clearly one in which $a-b>J$, where a and b are the Zeeman energies of the Yb^{3+} ion and the electron. This case has been evaluated explicitly by Van Vleck.[33] Thus, the 30% loss on signal at 1.5°K is attributed to those Yb^{3+} which have exchange interactions with the electrons. The 30% figure compares favorably with the 40% figure obtained for Gd^{3+} at 1.5°K.

The increasing relaxation rate of those Yb^{3+} which gave a resonance in the converted sample is attributed here as in the Gd^{3+} to long-range interactions between the dopant and the electrons.

V. OPTICAL AND ELECTRICAL EXPERIMENTS

A. Optical Techniques

The optical-absorption spectra were measured in the visible by a Cary 14 spectrometer, and in the near infrared (4000→400 cm^{-1}) by a Cary 90 spectrometer. The far-infrared measurements were made at R.C.A. by Dr. D. R. Bosomworth using a Michelson interferometer. The techniques used for this latter measurement are thoroughly discussed in Dr. Bosomworth's recent publication.[39] The visible and near infrared were measured in transmission at low temperatures using a conventional brass Dewar with a copper cold finger. The cold finger had a $\frac{3}{8}$-in. hole for the light to pass through. The sample was glued on the cold finger using Ge 7031 varnish. The windows of the Dewar were made of KBr, whose reststrahlen absorption extends from 25 to 40 μ. Spectra were taken on samples both before and after conversion so as to isolate the effects of the change to the semiconducting state.

The spectral response of the converted samples when used as photodetectors was measured in the near infrared by use of a 12-C Perkin Elmer spectrometer with a Bausch and Lomb grating (75 grooves/mm, blazed at 12 μ). In the visible, 0.4 to 1.6 μ, measurements were made using conventional Bausch and Lomb gratings with the appropriate blaze. In the intermediate regions various narrow-band filters were used. For most of these experiments a glowbar light source was used with the intensity of the light incident on the sample being measured by use of a calibrated Epley thermocouple.

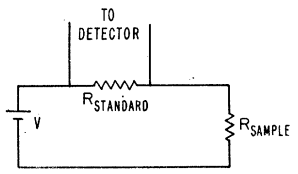

FIG. 10. Detection circuit of photoconductivity.

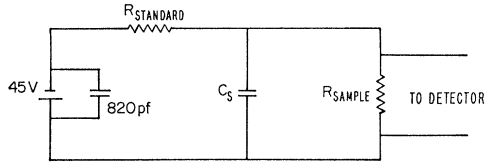

FIG. 11. Circuit used to measure time constant of photoconductive response.

B. Electrical Techniques

The photoconductive response of the converted samples was detected in most instances by use of the circuit shown in Fig. 10. Light incident on the sample would lower its resistance, thereby increasing the voltage across the standard resistor. This change would be detected by some high-impedance voltage detector which when phase detection was used was a P.A.R., either model J-5 or HR-8. For maximum sensitivity the standard resistor should have the same resistance as the semiconducting sample. This is seen in a straightforward manner by use of the circuit equation and simple differentiation of the expression for the change in voltage across the standard resistance as a function of the change in resistance of the sample. For practical reasons measurements were not always made under these conditions; however, the results will be labeled according to the V, R_{standard}, and R_{sample} used. For the photoconductive measurements leads were attached by indium sodder on the opposite faces of the rectangular samples. When important, the area of those faces as well as the thickness of the sample will also be specified. The measurements were made at helium temperatures in a Dewar of the type previously described (Sec. VA) or in a glass Dewar in which case the sample was immersed in helium.

The time constant of the photoconductivity sample was measured using a CO_2 and a Ruby laser (10.6μ) with the detection circuit shown in Fig. 11. The capacitance C_s arises from the stray capacitance of the leads to the sample which was in the Dewar.

C. Optical Measurements

The absorption spectra of various doped but unconverted samples were measured from 50 000 to 10 cm^{-1}. Their spectra was identical with that obtained for pure CdF_2 except for very small absorptions characteristic of the trivalent dopant. Those absorptions are small compared to the effects we will describe and play no role in the phenomena being studied. The gross features of the absorption of pure CdF_2 are, as stated in Sec. I, a charge-transfer transition which begins at 50 000 cm^{-1} and a reststrahlen absorption centered at 250 cm^{-1}.[39] Over the rest of the spectrum the pure and unconverted doped samples were essentially transparent.

[39] D. R. Bosomworth, Phys. Rev. **157**, 709 (1967).

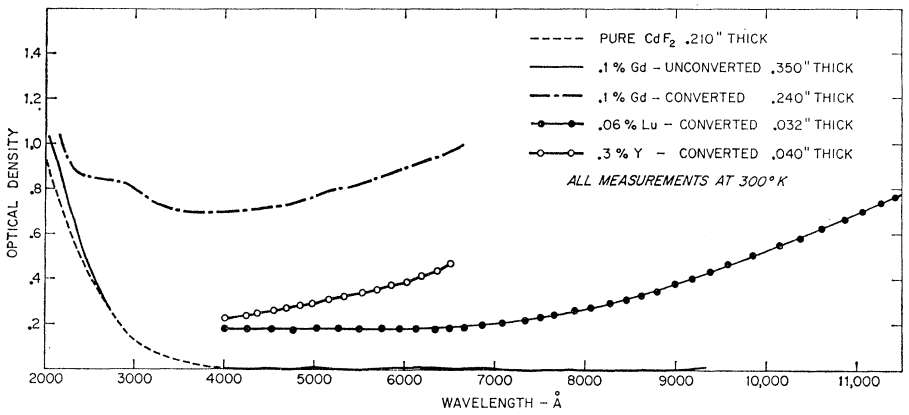

FIG. 12. Visible absorption spectrum—before and after conversion for various dopants.

For converted samples with doping concentrations higher than 0.05 mole %[15] it was found that their absorption was so strong from 20 to 10 000 cm^{-1} that no measurements could be made by the techniques described in Sec. V A. The tail of this large absorption in the visible is shown in Fig. 12 for various dopants. The growth of the absorption as one went further into the red went roughly at λ^3 as Weller[4] reported. The presence of a flat absorption in the visible is clearly indicated by the 0.1% Gd spectrum.[15] For 0.01% doped Gd and Nd samples[15] the absorption was measured in the near infrared as is shown in Fig. 13. The rising absorption at 600 cm^{-1} is the tail of the reststrahlen absorption band of the bulk crystal. The origin of the structure at 730 cm^{-1} is not known, but as seen in Fig. 13 it was present in pure CdF_2 as well as the doped and converted samples. The peak of the absorptions are at 1300 cm^{-1}, which corresponds very closely to the 0.16-eV activation energy obtained from Weller's data. The curves for the two dopants are quite similar as is evident from Fig. 13. In addition a 0.01% Yb sample[15] was measured in this region. The absorption was considerably larger than in 0.01% Nd and Gd[15] though the rise from 4000 to 2000 cm^{-1} as well as the beginning of the fall at 900 cm^{-1} was observable. The spectra for the Gd- and Nd-doped samples in this region were taken at 300°K as well as 77°K. The change in the two cases is small as is shown in Fig. 14.

The 0.01% Yb sample[15] was measured in the far infrared by Dr. Bosomworth. The preliminary results are plotted in Fig. 15. The sample has a strong absorption in this region as, of course, the higher doped samples also did.

D. Photoconductivity

By using the detection circuit shown in Fig. 10, photoconductive responses were observed at 4.2°K for 0.06% Lu, 0.3% Y, 0.1% Gd, 0.06% Tb, 0.01% Yb, 0.01% Gd doped samples.[15] The following properties of the response were determined by simple experiments.

(*i*) *Contacts.* The response is not due to absorption of light at the contacts with the subsequent injection of carriers. This was easily shown by masking sample with a copper shield which was in poor thermal contact with the sample and which exposed only a small area of the sample, far from the contacts.

(*ii*) *Concentration dependence.* The response of the 0.1% Gd sample was 1000 times larger at 10.6 μ than that of a 0.01% Gd sample.[15] Each signal was detected under the condition that $R_{\text{sample}}=R_{\text{standard}}$. This difference is significant since the optical absorption of the

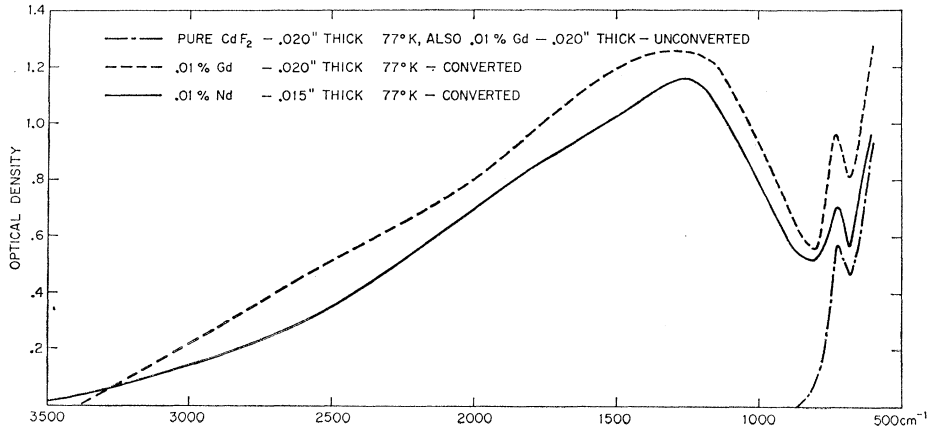

FIG. 13. Near-infrared spectrum — before and after conversion for 0.01% Gd and 0.01%Nd.

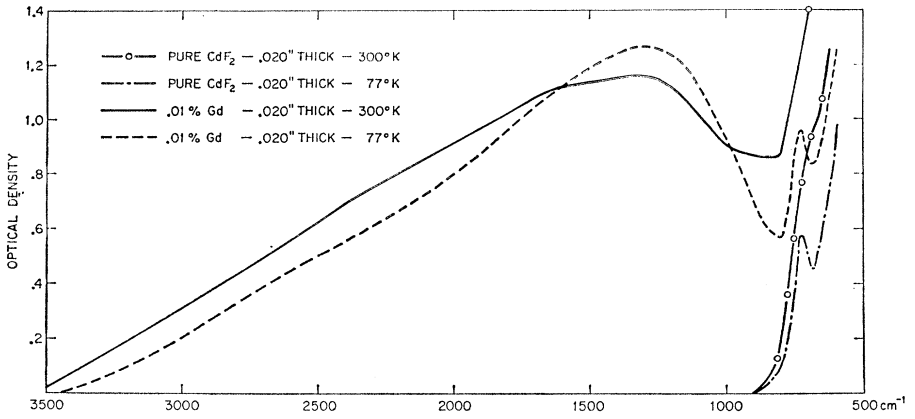

FIG. 14. Variation of near-infrared spectrum with temperature (0.01% Gd.)

0.01% Gd sample[15] at 10.6 μ (Fig. 13) was large enough so that all the light was absorbed, except for reflection losses, of course.

(*iii*) *Relation to absorption band.* The signal is related to the absorption band which appears upon conversion. For this experiment a thin (0.036-in.) and a thick (0.060-in.) 0.06% Lu converted sample[15] were studied in the visible where the absorption was finite (Fig. 5) and in the near infrared when it was complete. It was observed that in the visible (0.75 μ) the thick sample had a signal which was 2.1 times that of the thin sample, while in the infrared (5 μ) the ratio was approximately unity. Thus, the signal varied with the energy absorbed.

(*iv*) *Bandwidth.* Photoconductivity was detected as far as 20 μ into the infrared in 0.01% Lu, 0.03% Y, 0.006% Tb, and 0.01% Gd doped samples.[15]

(*v*) *Spectral response.* Using the thick Lu sample, measurements were taken at 0.64 μ, 5.34 μ, and 10.54 μ by using narrow-band filters. Using the Epley thermocouple the energy incident on the sample was measured in those ranges. The ratio of signal to energy was a constant within 10%. Beyond 12 μ no such ratio could be determined since the Epley was not sensitive enough to obtain a measurement of the input light in that region.

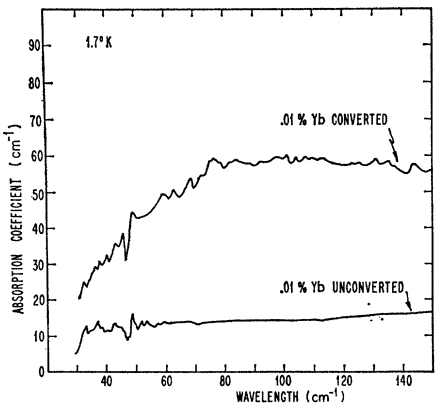

FIG. 15. Far-infrared spectrum of 0.01% Yb — before and after conversion.

(*vi*) *Time constant.* Measurements using the circuit shown in Fig. 5, a Q-switched CO_2 laser, and a 0.3% Y-doped[40] sample mounted on a cold finger, revealed that the response time was very sensitive to the temperature of the sample and therefore to its connection to the bath. A complex decay curve was observed which was characterized by two time constants. The initial fast decay had a time constant of 50 μsec. Measurements using a Q-switched attenuated Ruby laser with the sample immersed in helium showed that at 4.2°K the initial decay had a time constant of 15 μsec. At 1.3°K, a decay curve with a single characteristic time constant of less than 2 μsec was observed.

(*vii*) *Responsivity.* Using a helium-neon laser, 6328 Å, and a 0.3% Y-doped sample[15] immersed in helium with $R_{\text{sample}}=100$ k Ω and $R_{\text{standard}}=100$ k Ω, the responsivity was 40 V/W with a 25-V battery in the circuit shown in Fig. 10.

(*viii*) *Detectivity* (D^*).[41] Again using the helium-neon laser, chopped at 420 cps with a detection band width of one second, a 0.3% Y-doped sample[15] at 4.2°K, $R_{\text{standard}}=100$ k Ω, $R_{\text{sample}}=100$ k Ω, $V=40$ V and a surface area of 0.1 cm^2 a rough measurement of the specific detectivity yielded a D^* of 4×10^9 cm $(\text{cps})^{1/2}$ $(\text{W})^{-1}$. D^* is defined as the reciprocal of the noise-equivalent-power times the square root of the area band-width product.

(*ix*) *Thermal contact.* Thermal contact roughly equal signals were obtained when the sample was on the cold finger as when it was immersed in helium. The thermal contact on the cold finger could have been quite good so that the difference in connection to the bath may have been small.

(*x*) *Temperature dependence.* Using the normal detection circuit, the helium-neon laser, the response of a 0.3% Y-doped converted sample[15] immersed in helium was investigated as a function of temperature. Above 4.2°K the signal disappeared very rapidly. The results

[40] This sample was different from the one reported previously. P. Eisenberger and P. S. Pershan, Appl. Phys. Letters **10**, 248 (1967).

[41] J. A. Jamieson *et al.*, *Infrared Physics and Engineering* (McGraw-Hill Book Co., Inc., New York, 1963), p. 151.

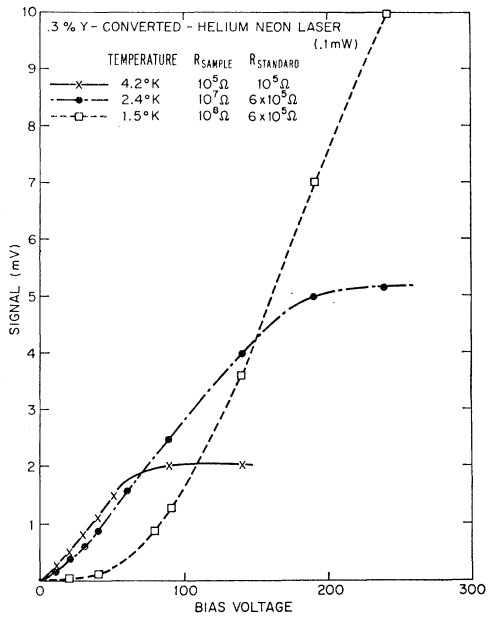

FIG. 16. Bias-voltage dependence of photodetector signal at various temperatures.

for 4.2°K and below are shown in Fig. 16. It should be noted that the lower temperature curves (2.4 and 1.5°K) were taken with R_{sample} not equal to R_{standard}. Thus, those signals are in fact larger than the 4.2°K signal. The second feature of those curves is the leveling off of the response at higher bias voltage V (Fig. 5). An indication that the response was sensitive to its connection to the helium was provided by a sharp rise and then fall in the response as the helium went into the superfluid state. This experiment was repeated many times and the transition was made in both directions.

E. Electrical Breakdown

As the bias voltage was increased above the point where the response leveled off electrical breakdown occurred. This phenomenon was investigated by itself. The following results were obtained.

(*i*) *Contacts.* The breakdown did not occur at a surface layer near the contacts to the sample. This was determined by investigating the breakdown electric field at 4.2°K in 0.06% Tb samples[15] of different lengths. Two samples whose lengths differed by a factor of 3 had the same breakdown field E_c of 460 V/cm.

(*ii*) *Concentration dependence.* Some other dopants and dopant concentrations were investigated. The results were: 0.3% Y, $E_c=275$ V/cm; 0.1% Gd, $E_c=250$ V/cm; 0.01% Gd, no breakdown observed $E_c>1500$ V/cm.[15]

(*iii*) *Temperature dependence.* As is obvious from Fig. 16, the leveling off occurred at higher voltages for lower temperatures. The increasing critical field with increasing resistance was qualitatively supported by other measurements.

(*iv*) *Repeatability.* The breakdown could be repeated many times with the critical field remaining the same for successive attempts. Thus no irreversible change in the sample seems to occur during breakdown.

All the above characteristics are compatible with an avalanche-type breakdown. This model would attribute the low-critical fields in the highly doped samples to the existence of low-energy electron traps from which electrons could be excited by the accelerating carriers. The existence of such low-energy transitions in the highly doped samples was indicated by the far-infrared results.

VI. INTERPRETATION OF RESULTS

A. General Optical Properties

Apart from the device possibilities of the system which will be discussed in the following section, the salient feature of the properties described in the previous section was the nature of the absorption which appeared upon conversion. The similarities shown in Fig. 13 between the Gd and Nd dopants and in Fig. 12 for various other dopants strongly suggests that it is the common trivalent characteristic of the dopants which is the important factor in determining the absorption and not their atomic properties. In other words, the ground and excited states of these "trapped" electrons do not contain a large admixture of the wave function of the divalent dopant. This is completely in agreement with the fact that except for Eu^{2+} no one has ever observed any divalent rare earths in CdF_2 under any conditions, including the ones described here.

The most naive interpretation of the near-infrared absorption (peaked at 1300 cm^{-1}) would be to postulate that the trapped electron moves in a hydrogenlike orbit about the trivalent rare-earth impurity.[4] This combination would be similar to the low-lying donor states in conventional semiconductors. One would thus expect the trap to be split off from the Cd^+ s-like band. Taking the effective dielectric constant $\epsilon=9$ and applying the Bohr equations one obtains values for the radius of the first Bohr orbit r, and for the binding energy E_b

$$r=4.75m/m^* \text{ Å}, \tag{6.1}$$

$$E_b=0.167m^*/m. \tag{6.2}$$

If $m^*\sim m$ the binding energy is in excellent agreement with the peak in the near-infrared absorption. The "radius" of the first Bohr orbit is very close to the length of the cubic unit cell (5.45 Å). Since the cell is fcc one could argue a spherical wave function would encompass approximately 8 cubic-unit cells. Thus the near-infrared absorption could be interpreted as transitions from the trapped state to the Cd^+, s-like conduction band. The extreme breadth of the absorption spectrum would have to do with either transitions to highly excited states in this band or to transitions to the next-highest conduction band, that is, the Cd^+ p-like band. Note that in atomic Cd^+, $E_{5p}-E_{6s}=3.85$

eV. If this is added to the postulated 0.16-eV trapping energy, this suggests an absorption edge at 4.01 eV or approximately 3000 Å. Thus the flat absorption in the visible might be due to excitonic-like transitions split off from the Cd^+ $5p$ band. A second possibility is that 3000 Å is the maximum, rather than the minimum, in this band.

The photoconductive effect in the near infrared would be perfectly consistent with this interpretation were it not for the fact described in Sec. V D, item (*vi*), namely, that the ratio of the photoconductive signal to the energy absorbed is constant, independent of wavelength throughout the region from 10.54 to 0.064 μ. Thus although the near-infrared absorption spectra can be interpreted in this way, there is an apparent inconsistency with the photoconductive response.

The resolution of this probably lies in the fact that the excited states for these near-infrared absorptions are probably very short lived. In fact one might expect that there are two time constants, one which would describe a very rapid decay of any excited electron to the bottom of the Cd^+ $5s$-conduction band and a second, possibly longer, time constant which describes the rate at which carriers get retrapped. Assuming this is true and noting that at the temperatures where photoconductive signals were measured the sample resistance had a 0.003-eV activation energy, it is not unreasonable to assume the decay to the bottom of the Cd^+ $5s$ band could very well excite some of these low-lying traps. This could come about directly, through an electron-electron scattering event or it could arise through a pure thermal effect, the decaying electron heating the lattice and raising its temperature. Possibly, even a combination of these two effects could be occurring. In view of the fact that a photosignal was observed, with visible light, when the detector was immersed in liquid He, [Sec. V D, item (*vii*)] it is not likely that this is due solely to a simple thermal effect.

The origin of the 0.003-eV activation energy for conductivity is not understood; however, we can offer some speculations. The electron-spin-resonance data very definitely required electrons to move between certain Gd^{+3} sites which were called the "second configuration." The subsequent discussion attempted to justify its existence. Possibly 0.003 eV is the activation energy required for an electron to hop between different groups of Gd^{+3} ions, that is, between two configurations of the "second" type or even between different types of configurations.

Although the justification for the existence of these configurations came from analysis of the EPR data, there is independent evidence for them. Figure 15 shows the far-infrared absorption of converted and unconverted 0.01% Yb sample[15] at 1.7°K. An electron within such a configuration would have a fairly high "local mobility" and for frequencies large compared to the reciprocal of the time it takes an electron to transverse this configuration it would behave as though it were free. That is, the temperature dependence of the high-frequency conductivity would be nil for the fraction of the electrons trapped in this type of configuration. Taking $\sigma(\omega)=c\epsilon^{1/2}(2\pi)^{-1}\alpha$, where $\epsilon\approx 9$, and from Fig. 15 ($\alpha=60$) one obtains a $\sigma(\omega)\approx 1(\Omega\ \text{cm})^{-1}$. This is of the same order of magnitude as the dc conductivity observed at room temperature and suggests that the only thing that has been affected by the temperature is the ability of the electron to move through the crystal, that is, to hop between rare-earth configurations. This is suggested by the concentration dependence of the photoconductive response (Sec. V D). For the same total power absorbed a factor of 10 decrease in concentration induced a factor of 1000 decrease in photoconductivity.

To estimate the size of these configurations, assume they can simply be approximated by a potential well. For simplicity we will assume an harmonic-oscillator type of potential for the well. However, the general result is not very sensitive to the form of the potential. It is a simple result that the frequency of the oscillator, or in quantum language, the energy of the $\Delta n=1$ dipole transition, is related to the amplitude of oscillation by

$$x=(\hbar/2\omega m^*)^{1/2}. \tag{6.3}$$

Thus for an effective mass equal to the free mass,

$$\omega=\hbar/2m^*x^2=1/2x^2. \tag{6.4}$$

The smaller the dimensions of the cluster, or potential well, the greater the energy separation between the various excited states. For our system the low-energy absorption at 30 cm^{-1} would correspond to configurations with 70 Å characteristic dimension while the peak absorption at 1300 cm^{-1} would correspond to only 9 Å. The latter dimension agrees quite well with the diameter of the hydrogenic-type orbit described. The analogy between the hydrogenic-like orbit and the harmonic oscillator model should not be taken too literally. We would like to consider the 30-cm^{-1} absorption as an "intraband" effect while the 1300 cm^{-1} should be an "interband" effect.

B. Photodetector

The fact that rare-earth-doped CdF_2 can detect infrared radiation is clear; however, the mechanism by which it does this is not so obvious. Certainly the trapped conduction electrons play a fundamental role in absorbing the infrared radiation, but we cannot yet say whether the same electrons which do the absorbing also contribute to the increased conductivity (i.e., as per the conventional photoconductor) or whether they simply heat the lattice and increased conduction results from increased temperature. It is even possible that some combination of these two may be going on. To the extent that CdF_2 is a thermal detector, its time constant would be a sensitive function of temperature, sample size, coupling to the bath, etc. In fact we have

observed some effects of these types; however, it still remains to do these measurements systematically. For example, photosignals were observed from a sample immersed in liquid He. This would tend to suggest that the detector may not be a thermal detector since, under these conditions, the sample temperature would not be expected to change much. Nevertheless when the sample temperature was lowered through the λ point, the photoconductor response showed an anomalous peak that would suggest coupling to the bath is an important factor.

VII. SUMMARY

The main goal of this work was to investigate the low-temperature state of semiconducting, rare-earth-doped, CdF_2. The ESR results, particularly for Gd^{3+} doped CdF_2, could only be explained in terms of an electron attracted to a trivalent rare-earth ion and held near it, although not on it, so that a divalent rate-earth ion is not formed. It was also necessary to postulate that although all of the electrons were trapped, in the sense that they could not contribute to the dc conductivity, some of them could move over sufficiently large distances as to interact with more than one rare-earth ion. The low concentration of rare-earth ions suggests that they (the ions) were not randomly distributed throughout the crystal but that some of them tended to form local regions of higher than average concentration. Far-infrared absorption measurements supported this suggestion.

Near-infrared absorption measurements revealed a broad band that peaked at 0.16 eV and was independent of rare-earth ions. Since Weller found that the thermal activation energy for carriers is also 0.16 eV the band has been associated with the ionization of electron traps. This is further supported by the observation of "photoconductivity" when near-infrared light is absorbed by these crystals. The properties of this "photoconductivity" have been discussed in Sec. VI B and we will not list them again. However, it is obvious that this is not a simple photoconductive process as one finds in conventional photoconductive detectors. In fact there is some evidence that part of this "photoconductive" effect may be a thermal effect; the electrical resistance of rare-earth-doped CdF_2 changing as the infrared radiation heats the crystal.

Further experiments in the near and far infrared are currently being undertaken in order to better understand both the "photoconductive" mechanisms and the electronic structure of these crystals. For the present, we claim the ESR experiments can only be explained in terms of the model discussed above and that the infrared and "photoconductive" behavior are consistent with that model.

ACKNOWLEDGMENTS

We would like to thank Dr. D. R. Bosomworth of the RCA Research Laboratories for taking the far-infrared absorption spectra and for allowing us to publish the preliminary data. We would like to thank Dr. R. Borscherts and Dr. J. Lambe for the open and illuminating discussion of their work. Helpful facts about the growing and conversion process were provided by Dr. J. D. Kingsley and Dr. J. S. Prenner. R. Callender helped with the photoconductivity measurements. We would also like to thank S. Maurici for help in cutting and polishing the crystals that were studied, and O. MacLeod for producing ohmic contacts on various samples.

APPENDIX A: g-FACTOR CALCULATION—POLARIZED WAVE FUNCTIONS

$$\epsilon\sum_{l=1}^{3}a_{jl}\Psi^{l}{}_{\mathrm{Cd}\ 5p}\text{—Eq. (4.3)}$$

Site	Wave function
110	$(\epsilon/2)[(\Psi_1^{-1}-i\Psi_1^{1})-(\Psi_1^{-1}+i\Psi_1^{-1})]$
$\bar{1}10$	$-(\epsilon/2)[(\Psi_1^{1}+i\Psi_1^{1})-(\Psi_1^{-1}-i\Psi_1^{-1})]$
101	$-(\epsilon/\sqrt{3})[\Psi_1^{0}+(\Psi_1^{1}-\Psi_1^{-1})]$
$\bar{1}01$	$-(\epsilon/\sqrt{3})[\Psi_1^{0}-\Psi_1^{1}-\Psi_1^{-1}]$
011	$-(\epsilon/\sqrt{3})[\Psi_1^{0}+i(\Psi_1^{1}+\Psi_1^{-1})]$
$0\bar{1}1$	$(\epsilon/\sqrt{3})[-\Psi_1^{0}+i(\Psi_1^{1}+\Psi_1^{-1})]$.

The other six sites are easily found from the above since inversion of the site correspond to the negative of the wave function (i.e., polarization is in opposite direction). The $\Psi_1^{0,1,-1}$ are the angular p functions:

$$\Psi^{0}=\tfrac{1}{2}(3/\pi)^{1/2}z,$$

$$\Psi_1^{\pm1}=\mp(3/2\pi)^{1/2}(x\pm iy). \tag{A1}$$

APPENDIX B: EXCHANGE INTERACTIONS BETWEEN TWO SPIN SYSTEMS

The Hamiltonian of interest has the general form

$$\mathcal{H}=a\sum_{i=1}^{N1}S_{1i}{}^{z}+b\sum_{j=1}^{N2}S_{2j}{}^{z}+\sum_{ij}J_{ij}\mathbf{S}_{1i}\cdot\mathbf{S}_{2j}. \tag{B1}$$

The case under consideration is when $J_{ij}>a-b$. The discussion in Sec. IV B showed clearly that it was necessary to divide the total moment of the system into two parts, one giving the transitions of the exchange-averaged signal and the other, those due to the fact that the moments a', b' were unequal. These conditions were stated in Sec IV B and we restate them below:

$$\tilde{\mu}^{+}+\mu'^{+}=a'S_1{}^{+}+b'S_2{}^{+}, \tag{B2}$$

$$[\tilde{\mu}^{+},\ \sum_{ij}J_{ij}\mathbf{S}_{1i}\cdot\mathbf{S}_{2j}]=0, \tag{B3}$$

$$\mathrm{Tr}[\tilde{\mu}^{+}+\mu'^{+}][\tilde{\mu}^{-}+\mu'^{-}]=\mathrm{Tr}[\tilde{\mu}^{+}\tilde{\mu}^{-}+\mu'^{+}\mu'^{-}]. \tag{B4}$$

From Eq. (B3)

$$\tilde{\mu}^+=\delta[S_1^+ + S_2^+]. \tag{B5}$$

A general definition for μ'^+ is

$$\mu'^+=nS_1^+ + mS_2^+. \tag{B6}$$

Using Eq. (B4)

$$\mathrm{Tr}[nS_1^+S_1^- + mS_2^+S_2^-]=0, \tag{B7}$$

or

$$m/n=-\mathrm{Tr}S_1^+S_1^-/\mathrm{Tr}S_2^+S_2^-$$
$$=-N_1S_1(S_1+1)/N_2S_2(S_2+1)=-\theta. \tag{B8}$$

From Eq. (B2)

$$a'=n+\delta,$$
$$b'=m+\delta. \tag{B9}$$

Using (B8) in (B9) one easily finds

$$\delta=(a'\theta+b)/(1+\theta), \qquad n=(a'-b')/(1+\theta),$$
$$m=-\theta(a'-b')/(1+\theta), \tag{B10}$$

which from Eqs. (B5) and (B6) results in

$$\tilde{\mu}^+=[(a'\theta+b)/(1+\theta)](S_1^+ + S_2^+),$$
$$\mu'^+=[(a'-b')/(1+\theta)](S_1^+ - \theta S_2^+). \tag{B11}$$

The ratio of intensities of the transitions caused by the two components of the moment is found by using Eq. (B11):

$$\mathfrak{R}=\frac{\mathrm{Tr}\tilde{\mu}^+\tilde{\mu}^-}{\mathrm{Tr}\mu'^+\mu'^-}$$
$$=\frac{(a'\theta+b')^2}{(a'-b')^2}\frac{[N_1S_1(S_1+1)+N_2(S_2)(S_2+1)]}{[N_1S_1(S_1+1)+\theta^2N_2S_2(S_2+1)]} \tag{B12}$$

or

$$\mathfrak{R}=\frac{[a'(\sqrt{\theta})+b'/(\sqrt{\theta})]^2}{(a'-b')^2}. \tag{B13}$$

For two spin systems of equal spin and number of particles ($\theta=1$)

$$\mathfrak{R}=(a'+b')^2/(a'-b')^2, \tag{B14}$$

which for a' considerably different than b' can even for large J ($J>a-b$) result in considerable intensity in the broad signal. For $\theta\gg1$ or $\theta\ll1$, $\mathfrak{R}$ is large and much less sensitive to $a'-b'$. This is reasonable since for extreme values of θ the total system's properties are mainly like one of its two constituents.

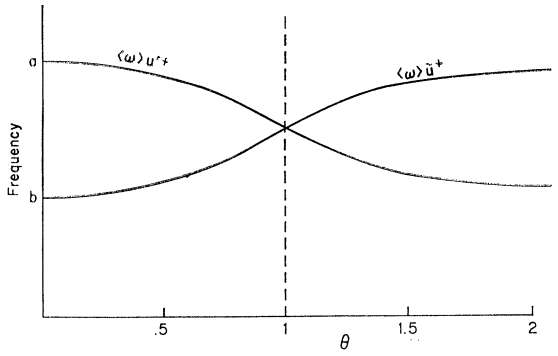

FIG. 17. Average frequencies of the two types of transitions as a function of the ratio of the intensities of the two spin system.

The mean frequency of the transitions due to $\tilde{\mu}^+$ is given by

$$\langle\omega\rangle_{\tilde{\mu}^+}=\mathrm{Tr}\tilde{\mu}^-[\mathfrak{IC}_1\tilde{\mu}^+]/\mathrm{Tr}\tilde{\mu}^-\tilde{\mu}^+$$
$$=(a\theta+b)/(1+\theta), \tag{B15}$$

while those due to μ'^+

$$\langle\omega\rangle_{\mu'^+}=(a+b\theta)/(1+\theta). \tag{B16}$$

For $\theta=1$, equivalent spin and number of particles, the two distributions are centered at the same frequency, $(a+b)/2$. However, as θ becomes large or small the two distributions separate as shown in Fig. 17.

It is interesting to note that the division of the moment as described above indicates clearly how the Hamiltonian itself can be divided so as to clearly distinguish the two types of effects. Our Hamiltonian can be rigorously rewritten as

$$\mathfrak{IC}=\frac{a\theta+b}{1+\theta}(S^z+S^z)+\frac{(a-b)}{1+\theta}(S_1^z-\theta S_2^z)$$
$$+\sum_{ij}J_{ij}\cdot\mathbf{S}_{1i}\cdot\mathbf{S}_{2j} \tag{B17}$$

or symbolically as

$$\mathfrak{IC}=\mathfrak{IC}_0+\mathfrak{IC}_p+\mathfrak{IC}_{\mathrm{exch}}. \tag{B18}$$

In this form

$$[\mathfrak{IC}_0, \mathfrak{IC}_{\mathrm{ex}}]=0,$$
$$[\mathfrak{IC}_{\mathrm{ex}}, \mathfrak{IC}_p]\neq0,$$
$$[\tilde{\mu}^+, \mathfrak{IC}_{\mathrm{exch}}]=0. \tag{B19}$$

However, the mean of $\mathfrak{IC}_p$, given by

$$\bar{\mathfrak{IC}}_p=\mathrm{Tr}\tilde{\mu}^-[\mathfrak{IC}_p, \tilde{\mu}^+]/\mathrm{Tr}\tilde{\mu}^-\tilde{\mu}^+, \tag{B20}$$

is easily shown to be zero. Thus, even though the separation of the Zeeman energy into two terms is completely arbitrary, the separation indicated above allows one to proceed with the whole analysis as if the two systems had identical spin and number of particles. In this context, the effect of exchange is now clearly seen as the removal of the effect of $\mathfrak{IC}_p$ by averaging it to its zero mean.